Antti Kuhlberg

# Assembling and Exploring a Small Radio Telescope

## Acknowledgements

I want to thank my instructor, Thierry Baills, for his animated and passionate teaching style that got me interested in his radio techniques classes. Also his support and professional insights regarding this study were an enormous help. I also want to thank Päivi Haanpää at the Helsinki Observatory for giving me the opportunity to work with the SRT and letting me use the University premises during the assembling of the SRT system.

There are several people who helped me during this process and during my studies in general: Tero Hokkanen, Henrik Vesterinen, Petri Kirves, Ismo Väänänen, Tuomas Pylkkänen and Teemu Mahrberg. I thank you all. With your support it has been a bed of roses – a real pleasure cruise.

I would also like to thank my wife and parents and all the lecturers at Metropolia who have corrected my mistakes, which I've made a few.

A special mention goes to Taneli Mäkelä. Niice!

This was done together. We are the champions, my friends.

In Helsinki on 28 March 2014

Antti Kuhlberg

| Author(s) Title | Antti Kuhlberg Assembling and Exploring a Small Radio Telescope |
|---|---|
| Number of Pages Date | 27 pages + 10 appendices 28 March 2014 |
| Degree | Bachelor of Engineering |
| Degree Programme | Electronics |
| Specialisation option | |
| Instructor | Thierry Baills, Senior Lecturer |

The subject of this study is a Small Radio Telescope (SRT), which is a radio astronomy kit for radio astronomers and students. In the course of this study, the SRT was set up and made available to the Helsinki Observatory.

The work on this study started by getting acquainted with the functioning of the SRT, gathering the necessary schemes and making sure that all the necessary components to set up the SRT were available. The different components were carefully tested before starting the actual assembling, which meant that hands-on work was needed throughout the process.

The task of making the SRT system operational and ready for future observations was successful. This thesis also serves as an introductory brochure for future SRT users, where the fundamentals of radio astronomy as well as the SRT system are explained step-by-step. Finally, receiver properties and the low-noise amplifier and band-pass filter are explored in more detail.

The block diagrams relating to the testing of the SRT parts are presented in the appendices as well as the schematics and assembly instructions.

| Keywords | Radio astronomy, SRT, filter, receiver, LNA, BPF, superheterodyne, RF, noise, SNR |
|---|---|

Helsinki Metropolia University of Applied Sciences

**Contents**

Helsinki
**Metropolia**
University of Applied Sciences

Appendices

## Abbreviations

AZ/EL        azimuth-elevation

BPF           band-pass filter

LNA          low-noise amplifier

LO            local oscillator

RF            radio/wireless communication

SNR          signal to noise ratio

SRT          small radio telescope

VLA          Very Large Array

# 1 Introduction

This study explores a Small Radio Telescope (SRT) belonging to the Helsinki University Observatory where the SRT telescope is located. The Observatory was designed by Architect C. L. Engel and Professor of Astronomy F. G. W. Argelander. It was built in 1830's and has contributed in various forms in the field of astronomy, including teaching and observations. Probably the most well-known and certainly the most laborious work, in the form of man hours, that Helsinki Observatory was involved with, was the international Carte du Ciel project. This project started in 1887 and combined the resources of twenty observatories around the world in an attempt to catalogue and map out the positions of over four million stars [17]. Today the Observatory works under the Department of Physic. It is part of the Helsinki University Museum and it venues exhibitions about astronomy and history of astronomy for school children and tourists alike.

In the beginning of this project, the telescope was not in operation because it was dissembled during the restoration project of the University premises. In order to serve the needs of the observatory, the preparations for this study included making the radio telescope operational.

The purpose of this study is to provide information for Observatory staff and other interested users at Ursa, regarding the basics of radio astronomy and the functions and operations of this particular radio telescope, with special focus on its receiver properties. The main research questions are:

- What is radio astronomy?
- How does the SRT function technically?
- What are the components of the SRT?
- What are the characteristics of a radio astronomy telescope receiver?

Providing answers to these questions forms the structure of this study. First basics of radio astronomy and the basics of the SRT system are explained. Then, the receiver is described in closer detail. After this, the reader is introduced to the process of testing the low-noise amplifier and the band-pass filter.

## 2  Basics of Radio Astronomy

### 2.1  The Jansky Unit

The optical region was for a long time the only part of the electromagnetic spectrum that astronomers took advantage of. In 1932, Karl Jansky, examining the interference caused by lightning storms, discovered by chance the noise that was sent by the Milky Way. After that, radio astronomy has developed gradually into an important part of astronomy [14, p. 255].

In radio astronomy the incoming signals are often very weak. When measuring different apparent radio sources strengths, radio astronomers use flux unit, which is called jansky (Jy). One jansky is equivalent to $10^{-26}$ watts per square metre per hertz. To give an example, a mobile phone in the moon emitting 1 watt power to all directions, would be measured on earth as a $5*10^{-19}$ watts per square metre. A radio astronomy observer on the Earth's surface would see this as a strong radio source. For example if a mobile phone, which operates in a 200 kHz wide band, is placed in the Moon the observer on Earth will perceive it as 250 jansky. However, in real-life radio astronomy observations, the flux density in strong signals is typically tens of janskys and in weaker sources only milli janskys (mJy) or even less [8, p. 245].

While the SRT is not capable of such accurate measurements, the fundamentals are still the same. Radio astronomy equipment must be able to measure very weak incoming signals and separate those from harmful manmade emissions.

### 2.2  Hydrogen Line

In this study, the frequency in which observations are made is 1.42 GHz, which is probably the most important frequency in radio astronomy. One of the reasons is that the emissions of the radio sky that are observed by radio astronomers are not the light from the stars, but radio waves from the gas and dust clouds that are remnants of supernova or star explosions. The 21 cm hydrogen line has been used to chart the structure of our galaxy, known as the Milky Way. The 21 cm hydrogen line is in fact one of the most precisely measured physical properties [13, p. 312].

## 2.3 Electro Magnetic Waves

### 2.3.1 Signals from Space without a Wire

When looking up at the stars at night, with the naked eye or with the world's largest telescope, our eyes receive radiation from the stars. This visible radiation is what we call light.

The radio astronomer observing the stars with a radio telescope receives radiation known as radio waves instead of visible light. Although more complex instruments than the naked eye are needed for analyzing these radio waves, the observer of radio waves can build up a picture of the radio universe that is just as real a picture or a chart of any visible objects of the universe. The radio astronomer observes different frequencies of radiation known as the electromagnetic spectrum (Figure 1).
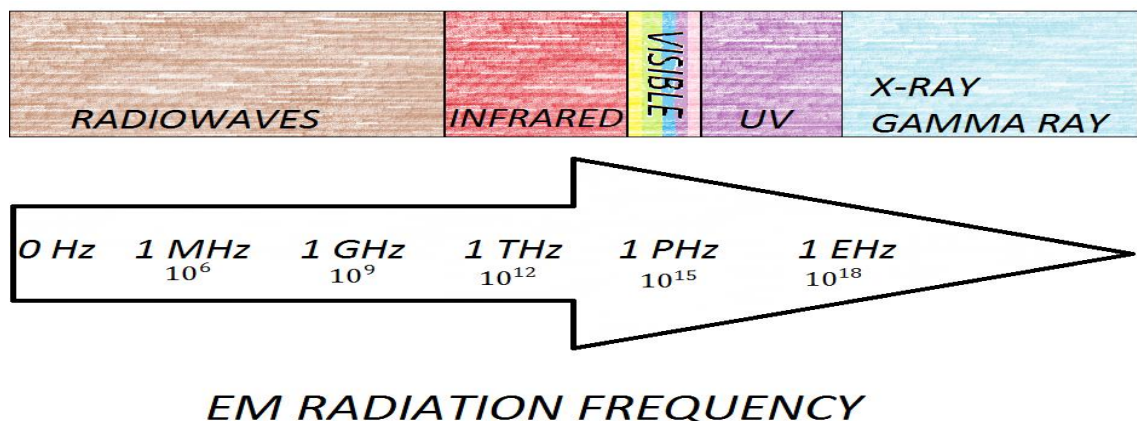


Figure 1. Different frequencies of the electromagnetic spectrum

### 2.3.2 Electromagnetic Spectrum

Maxwell, on the basis of the calculated speed of electromagnetic waves (EM waves), argued that light must be an electromagnetic wave. These so called Maxwell's equations were published in 1864 [14]. This idea was soon to come generally accepted when EM waves were experimentally detected.

Electromagnetic waves, or EM radiation, have been produced or detected over a wide range of frequencies. They are usually categorized as shown in Figure 1 above. The

figure is a rough model because the shifts, for example from radio waves to infrared, are not sharp in real life.

### 2.3.3   Two Windows to Space from the Earth's Surface

The EM radiation coming from space into our atmosphere comes from different sources, such as stars, planets, our own galaxy the Milky Way and black holes. The vastness of space is not fully known to man, which is why new objects and emitters can be found using the radio wave window. Different galaxies, for example, are very strong radio emitters, which is why radio astronomy has made progress in unraveling the mysteries surrounding the galaxies known as quasars. A quasar has an unusual spectral line. When combining the results from optical and radio wave astronomy, and with the help of redshift calculations, the quasar known as 3C273 was the first quasar ever to be identified. 3C273 was found in 1963 and it is still the optically brightest quasar in our sky. The most important qualities of quasars are their strong radiation levels and rapid changes in their brightness. Quasars are 100-1000 times brighter than the regular galaxies.

Different sources emit different kinds of waves. For example our own star, the Sun, sends a wide variety of EM radiation towards our planet. The Sun's EM radiation includes every radiation type listed in Figure 1 [6, p. 69].

Figure 2 demonstrates two so called windows that are transparent to incoming radio and visible optic waves. Black areas will be filtered out in the atmosphere and therefore never reach the Earth's surface. Because of this, should one wish to make observations on the Earth's surface, the windows that make observations possible are: the *visible* or *optic window* and the *radio window (*Figure 2)*.
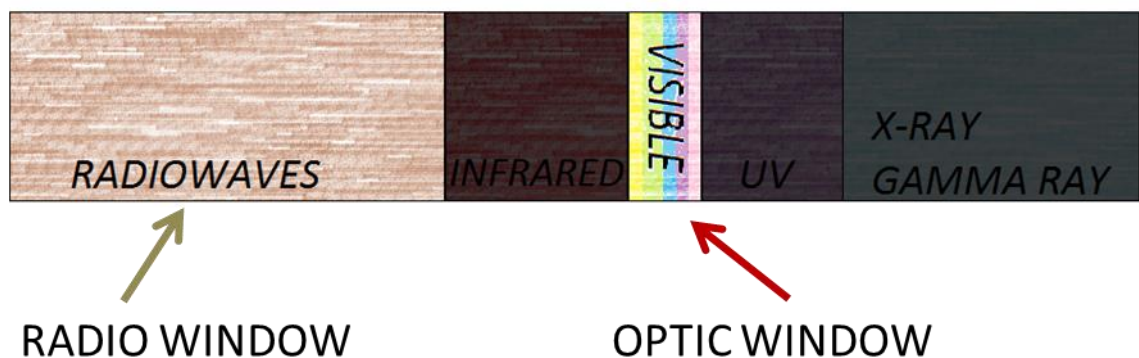
Figure 2. Only radio waves and visible -waves can penetrate the atmosphere

To give an idea; the *optic window* is roughly between [375 000 to 1 000 000] GHz (Giga $10^9$) and the *radio window* is between [0.015 to 1300] GHZ. [16].

These frequencies can also be seen as wavelengths, and it can be described as [5, p. 669]

$$\lambda = \frac{c}{f}$$

where $\lambda$ is the wavelength in meters, $c$ is the light speed in free space and $f$ is the frequency.

When moving in free space, the speed of EM wave is assumed to be fixed to the speed of light, denoted as **c**, which is 300,000,000 meters per second. Wavelength is then inversely proportional to frequency of the wave: the higher the frequency the shorter the wavelengths and vice versa [5, p. 325].

When seen as wavelengths, the λ for the optic window is between [800 to 300] nm (nano $10^{-9}$) where radio window is between [20 to 0.0003] meters.

2.3.4   Picking up the Wanted Radiation

The SRT device that is the focus of this study is designed to make observations in a specific frequency, which is 1.42 GHz, in the radio window (Figure 3).



Figure 3. Radio waves picked up by the SRT

Because of our blindness to radio waves, no naked eye observations can be made in radio astronomy. Therefore we have to rely on a man-made apparatuses to take a look through the radio window.

The wavelengths of radio astronomy are much (about one million times) larger than the wavelength of light, as noted above. This puts the radio astronomer in a difficult position, because the energy from radiation decreases as the wavelength gets longer. This involves great difficulty in achieving good resolving power compared to optical telescopes. To give an example, a 5 metre diameter optical telescope has the resolving power that is approximately 36 000 times greater than a 78 metre diameter radio telescope working in 300 MHz frequency at the Jordell Bank Observatory in Cheshire, England. [6, p. 216).

This is a problem that has been solved with a modern type of telescope known as the Very Large Array (VLA). The VLA consists of 27 independent antennas, each having a 25 metre diameter dish. The antennas are placed alongside in three 21 kilometres long lines. With the help of modern technology, it is possible to combine this wide array of radio telescope signals into one spot and make it work as one gigantic radio telescope antenna. This type of procedure is called aperture synthesis. The VLA works as an interferometer, which means that it operates by multiplying the data from each pair of telescopes together to form patterns and eventually chart the observations. Said VLA, called the Karl G. Jansky Very Large Array, located in New Mexico, operates as if it were a single dish system with one 36 kilometre diameter antenna [9].

## 3   Description of the SRT System

The SRT is a radio astronomy kit. It is designed for students and amateur observers interested in radio astronomy. It is designed to receive a 21-cm wavelength radiation, and the frequency in which observations are made is 1.42 GHz. The main parts of the SRT kit, as shown below in Figure 4, are

- the 2.3 metre diameter antenna dish,

- the mount for the antenna, which includes a gearbox and an actuator for moving the antenna,

- the receiver,

- the ground controller and the coaxial cables, and
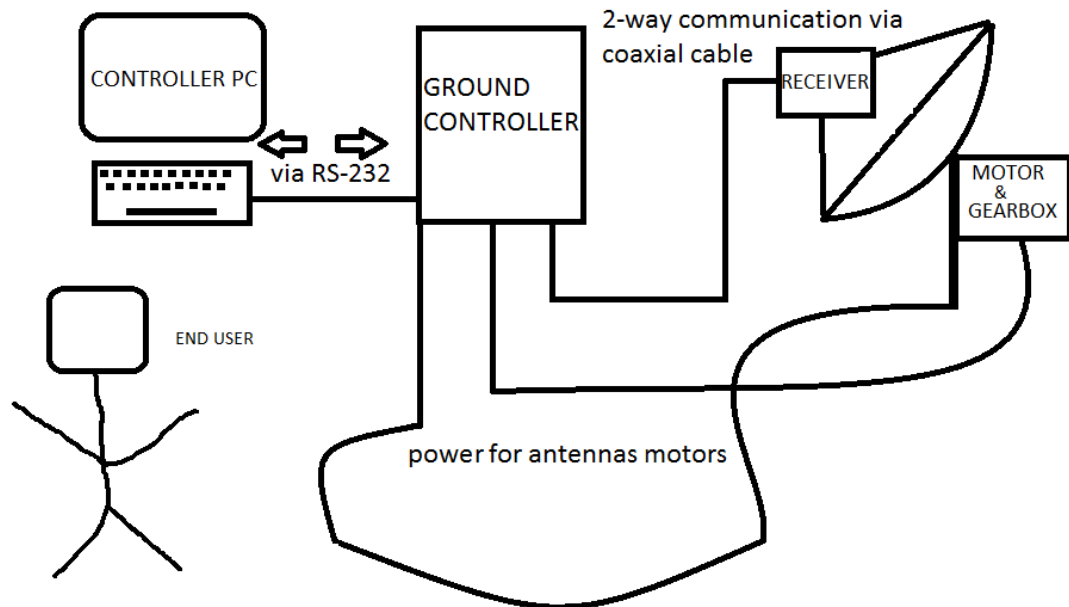
- the PC with a JAVA-based control software.



Figure 4. SRT mechanics

## 3.1    Antenna Basics

Antennas come in many different shapes and sizes. The antenna used for a mobile phone and the antenna used in a radio telescope are totally different in their uses and in their size as well. There are different criteria for characterizing them. In radio astronomy, essential characteristic of the antenna is its ability to distinguish signals coming from different directions. If the antenna could not give any indication of the direction of the signal, it would have no use in radio astronomy. The antennas in radio astronomy are said to be *directive*. Directivity is a measure how focused the antenna's radiation pattern is. In other words, directivity enables to get more power in to the telescopes receiver.

Every antenna has its own radiation pattern. Figure 5 below shows the differences in the radiation patterns of a parabolic antenna versus a dipole antenna. The picture shows how efficiently each antenna will receive EM radiation from different angles. Usually the pattern will contain a big main lobe and smaller side lobes. The radiation pattern can also consist of such angles from which the antenna does not receive any-

thing. Parabolic antennas used by radio astronomers will have better directivity than dipole antennas, because they are to receive signals from a fixed direction. In contrast, antennas for cell phones should have a low directivity because the signal can come from any direction, and the antenna should be able to pick it up [8, p. 139].
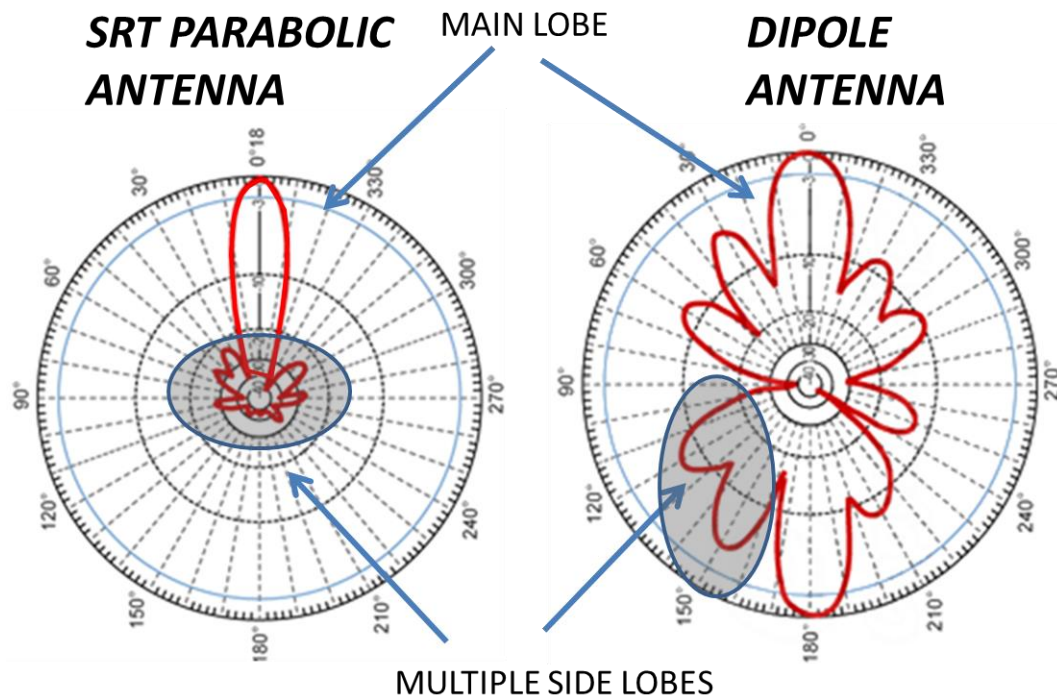


Figure 5.  Parabolic antenna and dipole antennas patterns [3]

If the antenna's physical size is smaller than the wavelength used, its main lobe will inevitably be wider than in a telescope with a much larger antenna compared to the wavelength used. This is the reason why radio telescope antennas are so colossal in physical size: they will use the size to get the telescope more directive.

*Gain* is another fundamental parameter. It describes how much power the antenna is transmitting from a source. An antenna with a 3 dB gain means that the power received by the antenna will be twice as much as what would be received by an antenna with a 0 dB gain. Furthermore, antennas that are small in relation to the wavelength at which they operate are usually very inefficient. A cellular phone has a gain of 0 dB, while the gain of a big radio telescope antenna can be as high as 40 to 50 dB [2].

The SRT uses a parabolic dish which is made of four individual sections. Each section is constructed from aluminum mesh supported by a lightweight aluminum frame, as seen in appendix 1. The holes in the mesh are seen as a mirror by the incoming waves, i.e. the holes will reflect the energy, if the holes are less than one tenth of the wavelength used. That is why the parabolic antenna can be made of lightweight aluminum mesh as shown in Figure 6 [6, p. 216). After reflected by the antenna, the wave is caught by the antenna feed (appendix 2). The antenna feed is located at the apex of the parabolic reflector.
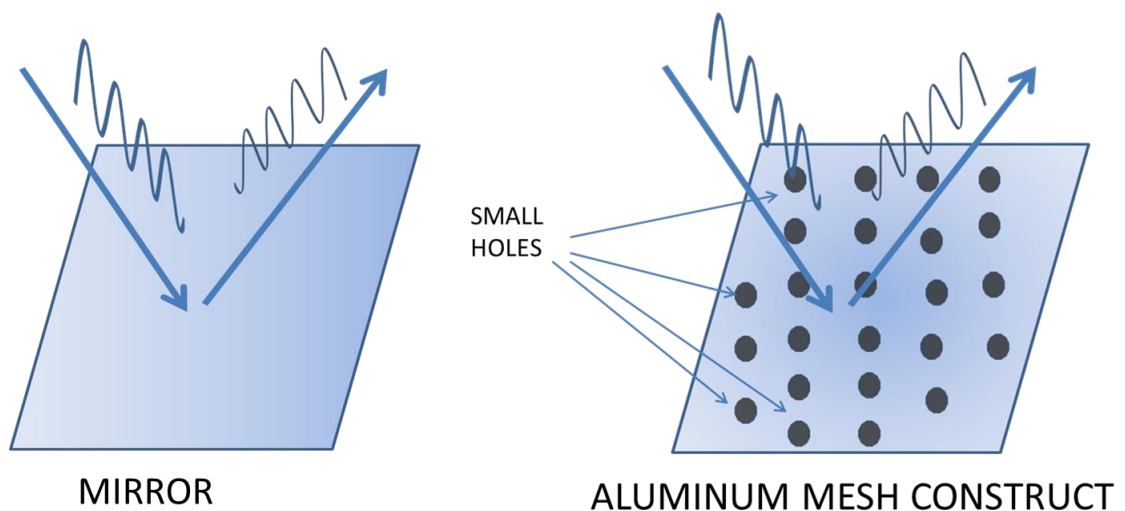


Figure 6.  An aluminum mesh construct working as a mirror reflector

3.2    Receiver Basics

The receiver can be described as the essential part of the system. It is a part where all the radio wave energy is concentrated. The incoming energy is physical power from radio waves, thus analog, and after the signal leaves the receiver, it is digitalized into bits. The block diagram and schematics of the receiver can be seen in appendices 4 and 5.

As mentioned earlier in Section 2.1, the incoming radio wave signals have very small power. The receiver needs to amplify that power without distorting it in the process. This is why the amplifying part will be of great importance.

The receiver itself always produces an unwanted and unavoidable noise signal which is of the same nature as the wanted signal. In other words, distinguishing between the

noise that comes from the receiver and the one that comes from sky is one of the fundamental issues in radio astronomy receivers.

## 3.3 Rest of the SRT Parts

### 3.3.1 The Ground Controller and Communications with PC

The ground controller provides the DC power to the antennas main motor gearbox, 2-way serial communication with the digital receiver on the antenna and finally it has an RS-232 serial port for connecting the software on user PC. The schematics for the ground controller can be found in appendix 7.

Communication between the ground controller and the PC is done using the RS-232 serial port. In many modern PC's the RS-232 port does not exist because of an invention we know as the USB port. In such cases the user will be able to manage by using a USB-to-RS-232 converter.

### 3.3.2 The Motorized, Two-Axis Mount

The Cassi mount is an azimuth-elevation (AZ/EL) mount that rotates the antenna in two axes; vertical and horizontal. These instructions can be found in appendix 3. The vertical altitude movement is done by a linear actuator attached to the antenna's frame, which operates with 24V DC supplied by the ground controller. The horizontal movement is done by the motor, with the needed 24V DC again supplied by the ground controller that rotates the motor gearbox located on top of the mast, just under the antenna itself.

The main motor gearbox assembly (Figure 7), where all the power connections from the ground controller unit are located, weighs 70 kilograms and has a reed micro switch attached to its worm gears in order to keep track of the turnings of the drives, and that way keep track of the antenna's position. The motor activates when it receives the keyword "move" from the ground controller. The keyword is followed by a byte which gives the number of "counts" of the reed micro switch on the drive gear to move [10].

ANTENNAS SUPPORT FRAME
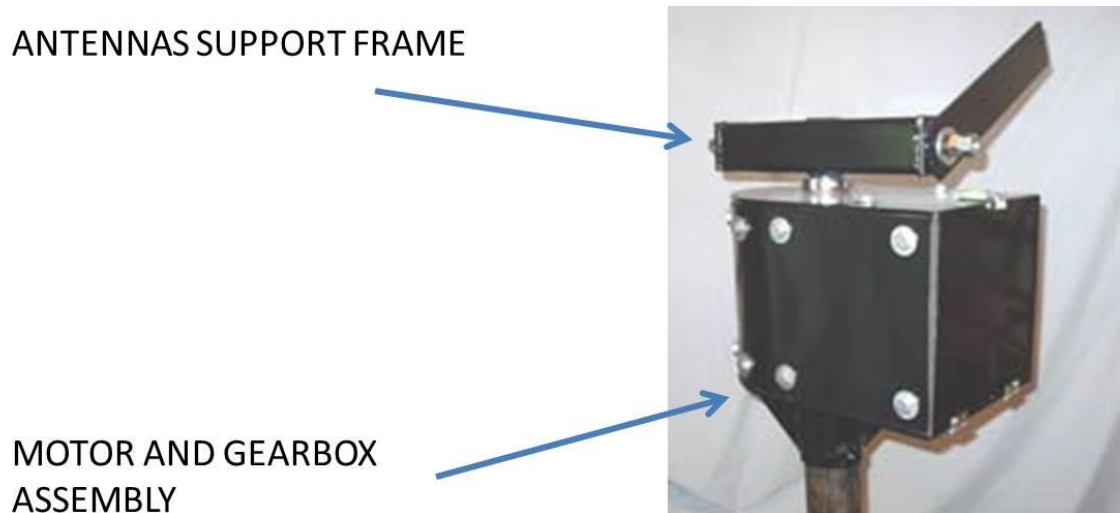
MOTOR AND GEARBOX
ASSEMBLY

Figure 7. The SRT mount and gearbox [1]

### 3.3.3 PC and Control Software

The control software, which is JAVA-based, was obtained from the MIT Haystack Observatory website. Being JAVA-based, the software is portable to most common operating systems. Interface for the telescope control is an active window and with that the user can control the telescope functions. Just like any other graphical user interface, the telescope functions are available either by a mouse clicking or typing text commands into text box. Also the combination of those two above methods are valid.

Before starting to use the SRT for the first time, the user needs to access an ASCII file labeled srt.cat. That file contains all the necessary information that the software is going to use, including telescope station latitude and longitude, telescope azimuth and elevation limits and the appropriated mount that will be used. The srt.cat file also includes the value for the noise diode calibration and ready co-ordinates for a few sky objects.

## 4 Focusing on the Receiver

The next part in the chain is the receiver. In a radio telescope the receiver plays a part that is similar to the photographic plate at the focusing point of an optical telescope. It is the point where the received electromagnetic waves are focused on and converted into bits, in order to be communicated to the user software and PC (Figure 8).
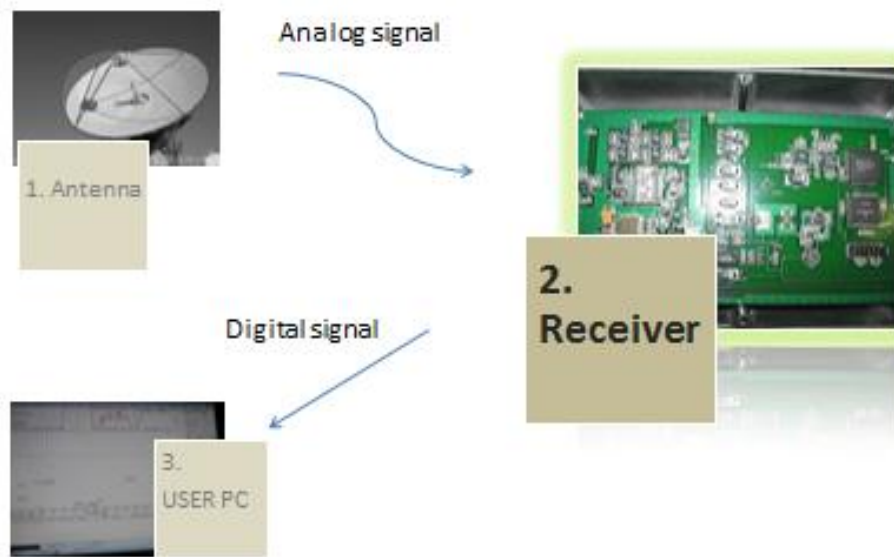
Figure 8. Signal path in SRT system

In order to select the wanted signal from any unwanted signals, we need selectivity. In most cases the power level of the signal a radio telescope receives is quite small and the power received from the background may be much higher than this. That is where the amplifying part and the sensitivity of the system will be of great importance.

Therefore the focus in this chapter is in the receiver's *sensitivity*, *selectivity* and internal *noise*. The reader should note that what is said of sensitivity, noise and selectivity is mainly true for any RF receiver. Also a closer look will be taken at the architecture of the SRT's receiver and its advantages in picking up the wanted signal.

4.1   Receiver Sensitivity and System Noise

As explained in Section 2.1 above, a mobile phone in the moon emitting 1 watt power would be seen as a very strong source for radio astronomy's observations on the Earth's surface. This illustrates how sensitive the receivers are in radio astronomy.

Receiver sensitivity is without a doubt one of the key specifications. The ability of the receiver to pick up the wanted radio signals as efficiently as possible is significant in any application. There are a number of methods and figures that are used to describe the receiver's sensitivity. This study concentrates on the following basic elements: signal to noise ratio (SNR), noise factor and noise figure and lastly noise temperature.

Noise can be defined as any random interference unrelated to the signal of interest [12, p. 37]. Unfortunately it is present in all circuits, generated by different components of the system; resistors, bipolar devices HEMT's. Basically every component wants to introduce its own noise into the system. Noise is very much the same hissing sound as can be heard from an amplifier with no output. Back in the day when there was no television transmission during the night, you could hear the same hissing sound with "snowflakes" on the televisions screen. The gentle hissing sound was generated in the systems own components. It presents a limitation on many aspects of performance.

Noise is something that is present in all electronic and RF circuits. Noise arises from many causes and sources. It originates from the movement of the charges. Electrons bump into each other continuously, the faster and the warmer the material is. This colliding will cause electrons to emit radiation. This radiation is what we call *thermal noise* and it is said to be white noise, which means it is not fixed to any one frequency but all frequencies [11, p. 232].

What makes matters complicated is the fact that in radio astronomy the noise is actually a useful signal. The fundamental challenge in radio astronomy is how to determine the unwanted noise from the wanted noise.

4.1.1   SNR or Signal to Noise Ratio

The signal-to-noise ratio (SNR) is an important parameter. The SNR can be defined as the ratio of the signal power to the total noise power. Mainly because of computational convenience, most of the receiver parts are characterized by their noise figure, which is expressed in decibels (dB). Figure 9 below demonstrates the noise created by the amplifier. The SNR is smaller after than before the amplifier.
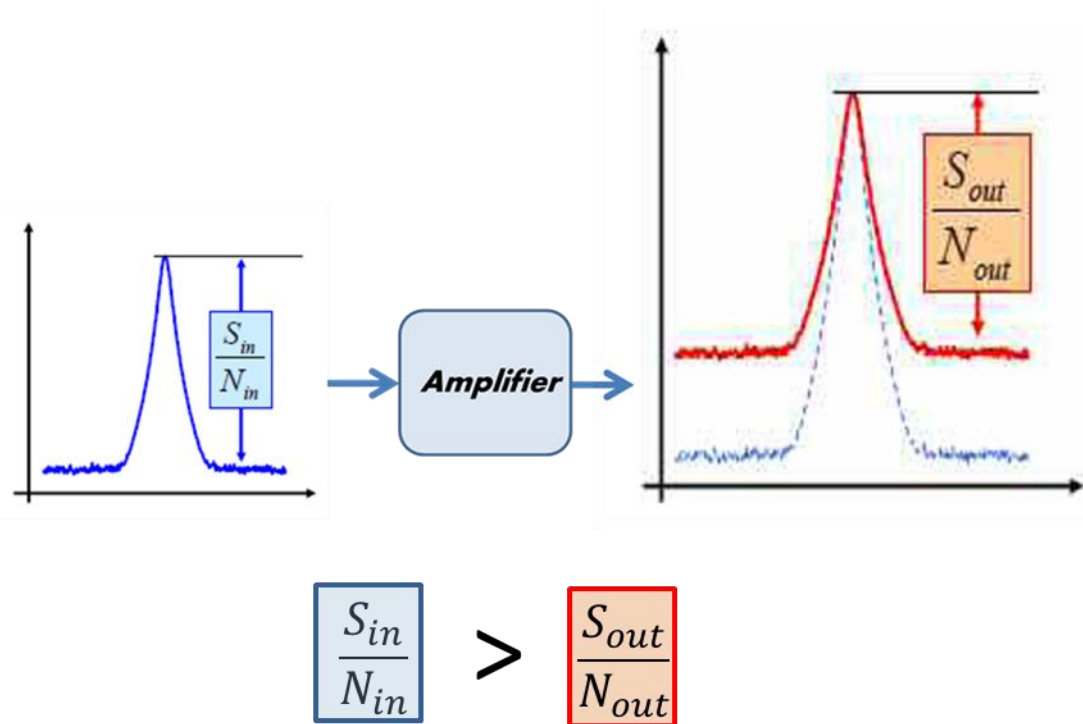
Figure 9. The amplifier introduces its own noise to the signal

4.1.2   Noise Factor and Noise Figure

In many analog circuits, the SNR is an important parameter to understand, but most receivers are characterized by their noise factor. The most common definition is [12, p. 39]

$$\text{noise factor} = \frac{SNR_{in}}{SNR_{out}}$$

where $SNR_{in}$ and $SNR_{out}$ are the SNR measured at the input and output.

To understand the physical meaning of the equation, noise factor can be seen as a figure of how much the SNR degrades as the signal passes through the system. A system that has no additional noise introduced, then

$$SNR_{out} = SNR_{in}$$

That means, in theory, the noise factor of a noiseless system is 1.

In reality, however, [12, p. 40]

$$noise\ factor\ > 1.$$

Noise factor was described in natural numbers. When defining the same in decibels (dB) we have [12, p. 40]

$$noise\ figure\ (dB) = 10\ log_{10}\ (noise\ factor).$$

So the figures compare the noise performance of a system to that of an ideal noiseless system.

How sensitive a receiver can be is directly proportional to the receiver's noise factor.

The receiver noise is usually expressed by the equivalent noise temperature $T_{receiver}$. It is the temperature to which the radiation resistance of the antenna would have to be raised in order to produce, the same noise power as the complete receiver [15, p.42].

### 4.1.3   Noise Temperature

Noise figure can also be defined as a Noise Temperature [7, p. 260]

$$noise\ figure = \frac{T_0 + T_{sys}}{T_0},$$

where $T_0$ is the reference temperature (usually 290ºK) and $T_{sys}$ is the temperature of the system.

In temperature terms; if the receiver is assumed perfect and introduces no noise, then

$$T_{receiver}\ = 0,$$

which equals

$$noise\ figure = 1.$$

The value of $T_{receiver}$ depends on the circuits and amplifying devices in the receiver.

The overall system temperature measured at the output of a receiver can be broken down as follows [7, p. 240]

$$T_{system} = T_{antenna} + T_{receiver},$$

where $T_{antenna}$ is antenna temperature, due to external radiation, partly from the sky and also interference from the ground and $T_{receiver}$ is noise temperature of the receiver.

This total noise temperature determines the sensitivity of the radio telescope system and also the receiver can be specified from standpoint of noise by its noise temperature $T_{receiver}$. In radio astronomy telescopes, the receiver sensitivity is of primary importance, because doubling the system noise temperature will extend the measurement period to four times [14, p. 257]. Also, the stability must be good.

## 4.2 Selectivity

Selectivity is one of the receiver's two main functions. One is to amplify the incoming signal and the other is to separate the wanted signal out of the unwanted ones. A receiver's ability to respond only to the wanted signal, or frequency or channel, and reject other unwanted signals nearby in frequency, such as Global Positioning System (GPS) and many different types of wireless communications done with cellular devices, is important one. Selectivity can be seen as one of the major specifications of any radio receiver for whatever application.

## 4.3 The Superheterodyne Receiver

The receiver in the SRT system is based on superheterodyne architecture. The term superheterodyning simply means creating a beat frequency that is lower than the original signal frequency (RF) captured by the systems antenna. The lower beat frequency is created by using the local oscillator (LO). The SRT uses a phase locked oscillator. It means that with the help of crystal, the LO is forced to oscillate at the frequency of the

crystal. The crystal is like a tuning fork whose resonant frequency remains constant. The RF signal of the receiver is mixed with the LO signal to form a lower intermediate frequency (IF) in order process the signal more easily. Basically this means adding two frequencies together in order to get one with lower frequency. When signal frequency has been reduced, the signal processing comes much easier. Figure 10 below illustrates how the downconversion is made.
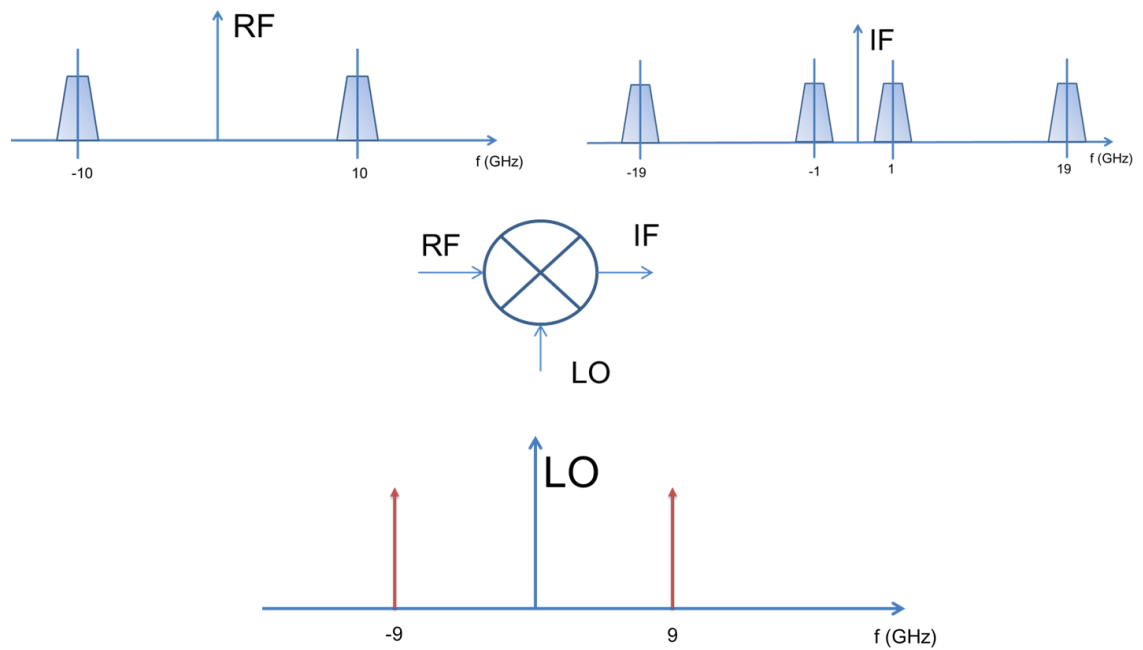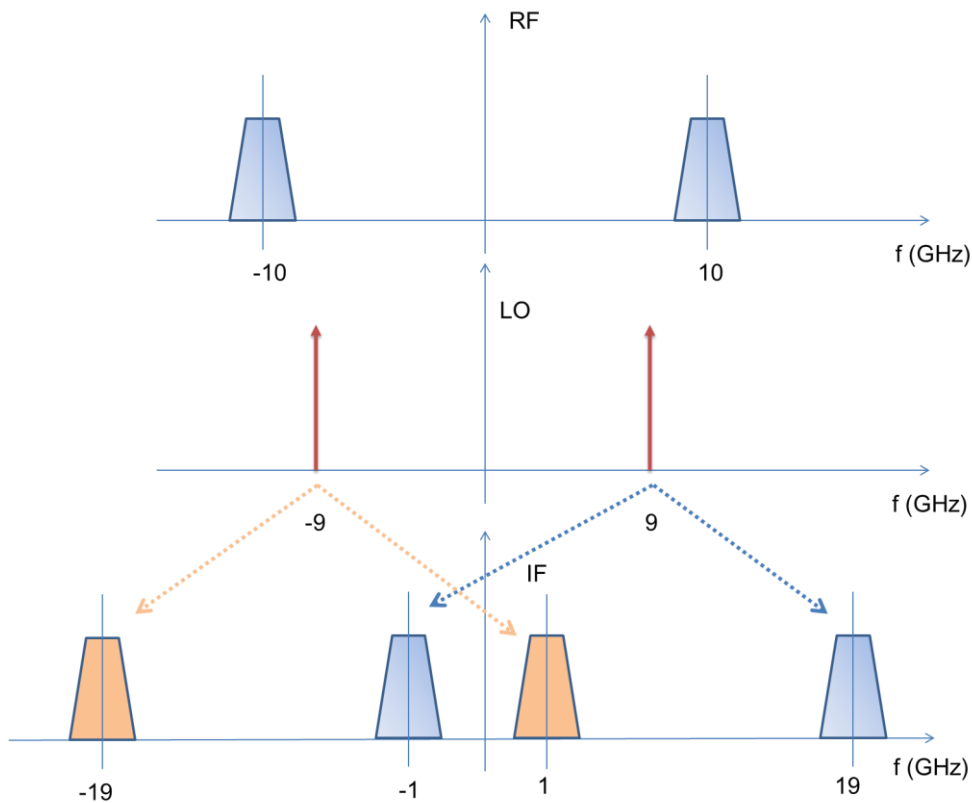
Figure 10.    Superheterodyning

### 4.3.1   Mixer

The mixer is a circuit in the middle, where the signal frequency is converted down-wards. For example, if a sinusoidal RF signal waveform contains 10 000 000 cycles, i.e. the signal frequency is 10 GHz and LO signal, has the frequency of 9 GHz, the IF frequency will be 1 GHz. So mixer forms a signal frequency that is the subtraction from RF and LO -signals 10 – 9 = 1.

The waveform that passes the switch is: (RF - signal waveform) x LO switching function.

In the SRT, the local oscillator must be set at a frequency that will "heterodyne" the original 1.42 GHz to the desired IF frequency of 0.5 to 3 MHz's, as seen in appendix 8. This means the local oscillator must be set accordingly so that the difference frequency will be in between the desired IF frequency range, which in SRT system is, 0.5 to 3 MHz's.

4.3.2   Advantages of a Superheterodyne Receiver

One of the main advantages of using a superheterodyne receiver is that it reduces the signal from very high frequency sources where components would not work properly. In SRT the observed frequencies are high at 1.42 GHz. Although in Metsähovi Radio Observatory in Kirkkonummi, which is much more sophisticated system, the telescope is capable of making observations up to 300 GHz. However, even when working with frequencies over 1 GHz, many ordinary components cease to function. For example, the most modern computer processors for PC systems work today at 3 GHz and there are many physical reasons for why the speeds are not in tens or hundreds of GHZ's. A superheterodyne receiver also allows many components to operate at a fixed IF frequency which helps the optimization and designing of the system.

Another advantage is that by using a superheterodyne receiver, it is very easy to improve the selectivity. In SRT receiver, as in television and in radio receivers, a user wants to tune the receiver into different channels or frequencies. So, besides sensitive, the receiver needs also to be selective.

## 5   Testing the Low-Noise Amplifier and the Band-Pass Filter

5.1   The Low-Noise Amplifier (LNA)

The performance of any radio telescope or any system that uses the RF is determined by both the power delivered to the antenna, bigger antenna equals more power gathered, and the sensitivity of the receiver, particularly the noise of the LNA. The noise temperature of the receiver is given by [7, p. 263]

$$T_{receiver} = T_1 + \frac{T_2}{G_1} + \frac{T_3}{G_1 G_2},$$

where $T_1, T_2 \ and \ T_3$ are noise temperatures and  $G_1$ and $G_2$ are the gains of each part.

Because the LNA is the first stage of gain in the receiver path, its noise figure adds directly to the noise figure of the system. This is the reason why it is important to put much emphasis on the LNA. The LNA schematics can be seen in appendix 6. Above mentioned equation can be used to find the noise temperature of the actual receiver when the noise temperatures and the available power gains are known.

A typical receiver having two RF amplifier stages followed by a mixer and an IF amplifier is shown in Figure 11 below.
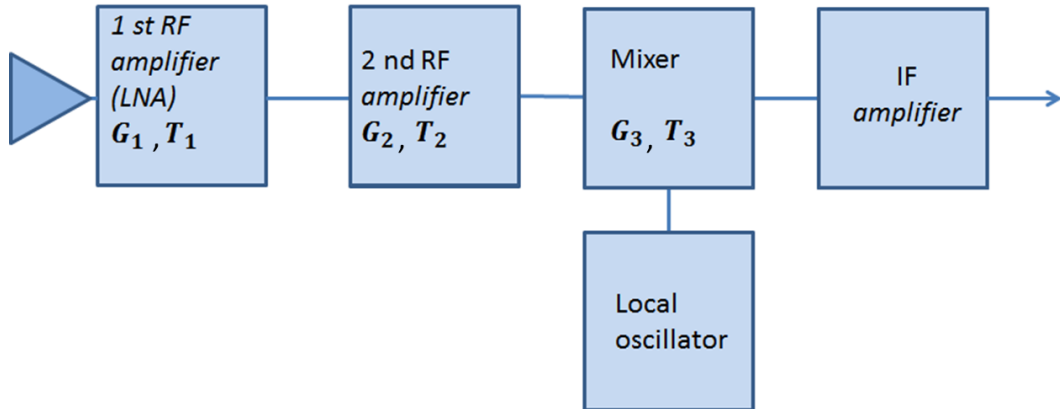


Figure 11.    Receiver path with two amplifiers

## 5.2   The Band-Pass Filter (BPF)

One simple method of minimizing noise in a system is to limit the frequencies that enter the system. This type of bandwidth limitation is done by using the band-pass filter (BPF), because when using a circuit bandwidth greater than that required by the signal, it allows additional noise frequencies to enter the LNA and rest of the circuit (Figure 12). The BPF will pass the wanted 1.42 GHz signal and provide good rejection for the unwanted frequencies. These unwanted interference frequencies come from many different sources. GPS, Personal Communications Service (PCS), different satellites and airborne transponder signals which are all operating in frequencies around SRT's 1.42 GHz hydrogen line. Thus, the 1.42 GHz is surrounded by interference from other systems and applications.  Also, when BPF adds very little noise on its own to the system itself, it will protect the rest of the receiver parts from unwanted, manmade interference, which is especially true in urban surroundings where the SRT is located [11, p. 134].
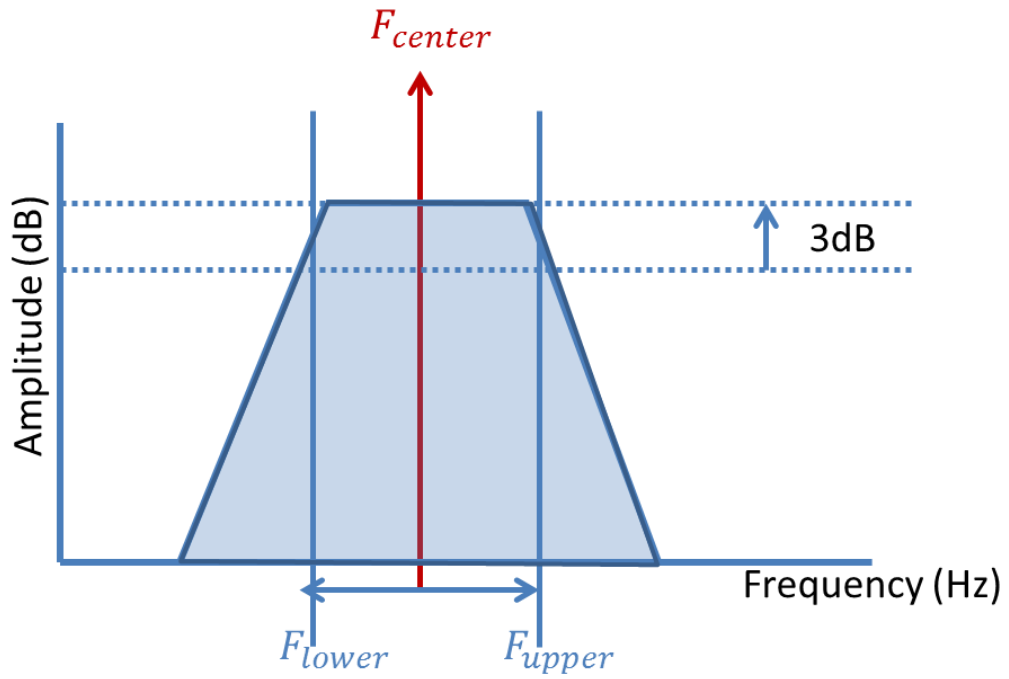
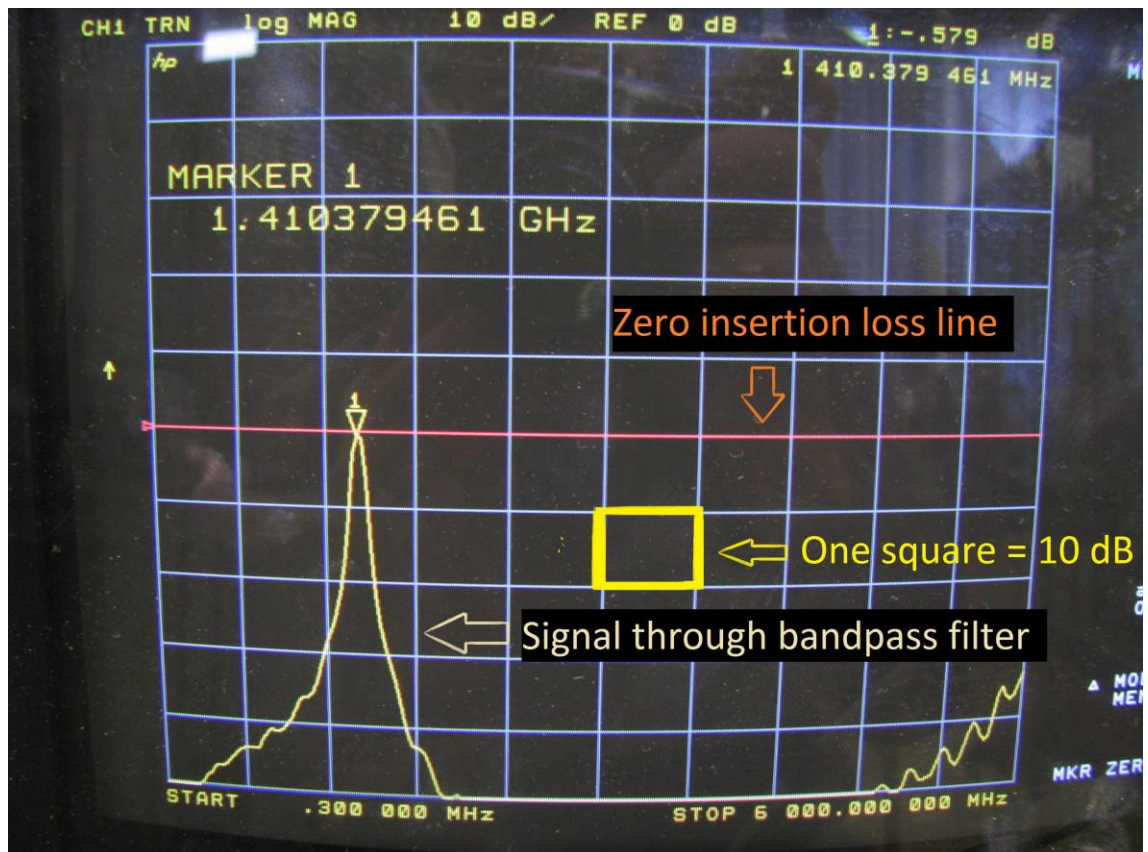Figure 12.    Band-pass filter attenuates frequencies outside its range



Figure 13.    BPF narrows down the bandwidth effectively

Figure 13 is from the network analyzer that has SRT's band-pass filter attached to it. It is a wide spectrum picture, just to enhance the BPF's role in the system. The spectrum is ranging from 0.3 GHz up to 6 GHz, from left to right. The yellow line at the bottom of the screen is our signal going through the filter. The red line in the middle of the screen is the level where there is no insertion loss which means those frequencies will pass through the filter without any obstacles.

Looking at Figure 13, the signal is seen peaking at 1.41 GHz where the filter makes no attenuation to the signal. This type of filtering is a very efficient way to limit the band-width and the noise entering the receiver.

The closer together the yellow and red lines are, the more of the original RF signal gets permitted through at that given frequency. As is evident from the peak, in this case only the specific signal frequency, 1.410 GHz, is permitted to go through.

5.3   Testing the Amplifier and the Filter

In SRT, the receiver is attached to the antenna mount, which means that it is located outdoors while the controlling PC is indoors. The cables and connections that the SRT system needs in order to work are then minimized. For example the LNA, which is attached next to the receiver, is powered by the +5V carrier through the coaxial cable.

When testing the LNA itself in the network analyzer, some arrangements needed to be made. Firstly, the LNA needed the 5V DC power for DC biasing and secondly, because of the outboard DC power used, a DC block connector (Figure 14) was needed because otherwise the dc signal coming from outboard power would have interfered with the network analyzers readings.
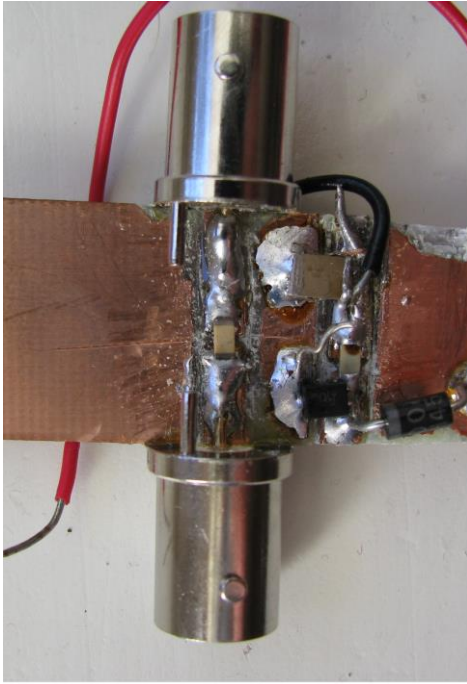
Figure 14.     DC block connector assembled in FR4 plate

After that, a block connector was simply made from two BNC connectors attached to FR4 plate. Then one 10 pF conductor was soldered to FR4 plate in between the BNC's and it was matched to 50 ohms using microstrip line calculator. EM Talk's Microstrip Line Calculator [4] was used in order to resolve the needed measures that the connector needed.

After the DC block connector the LNA was opened and 2 wires for +5V and ground were soldered in (Figure 15). Crude and robust in construct, but in practice the DC block connector worked soundly.
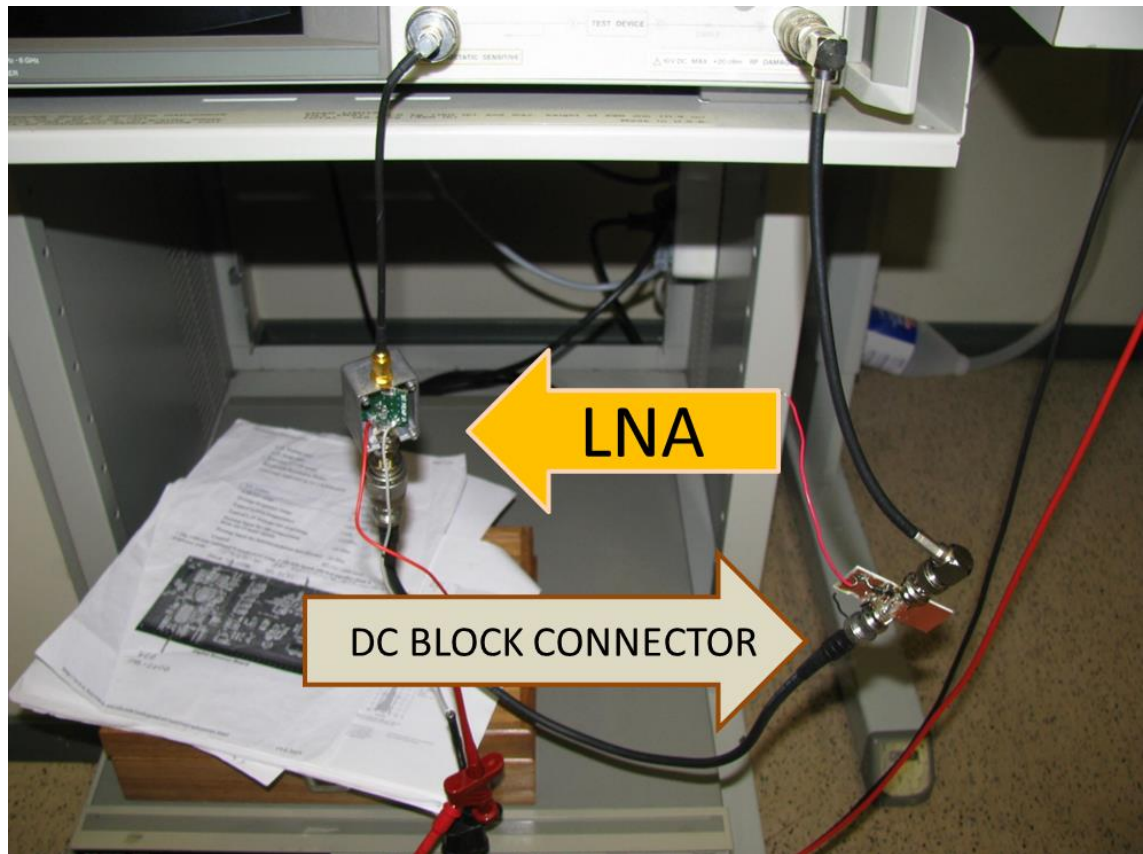
Figure 15.     Complete LNA setup in network analyzer with DC block connector.

After the setup was made, the LNA was put into test, which it passed nicely. Figure 16 demonstrates that the gain the LNA gave was 18.8 dB at 1.42 GHz, which was what the datasheet of the given ATF-34143 HEMT transistor said it would produce. The HEMT datasheet is attached here as appendix 9.
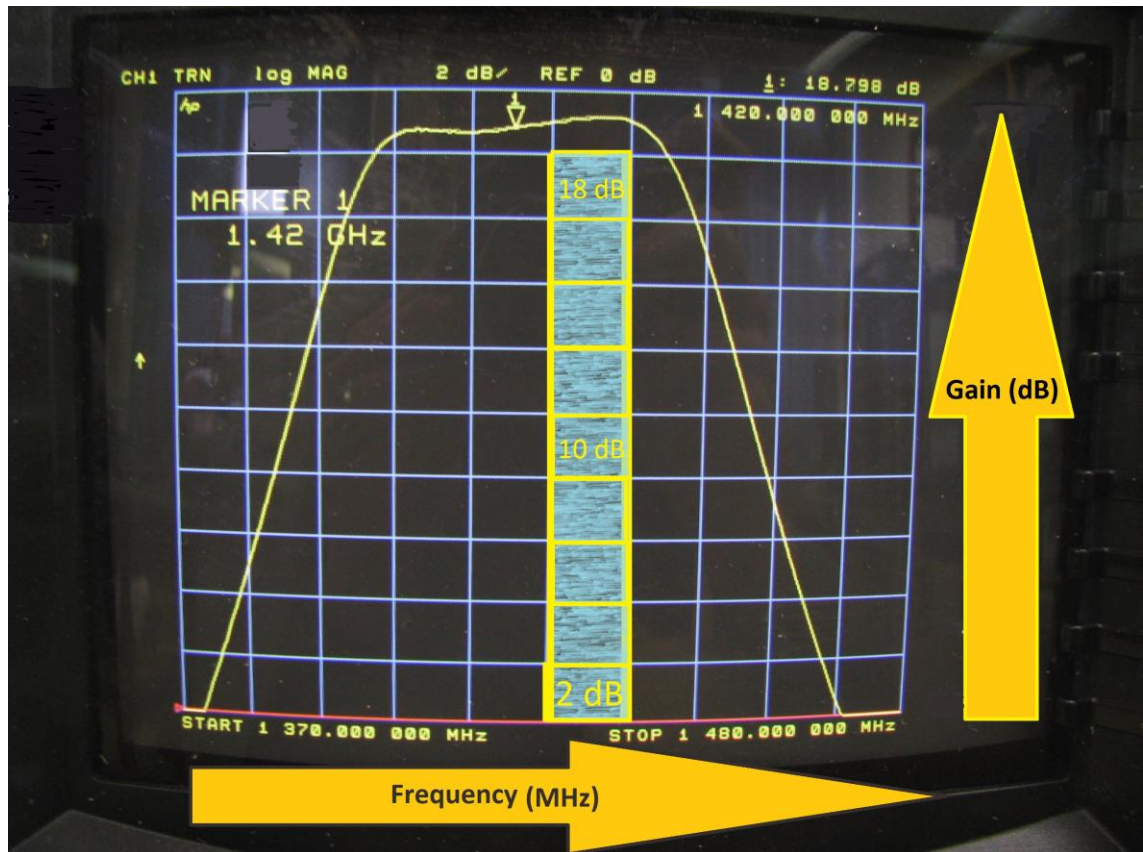
Figure 16.    LNA in network analyzer

## 6    Summary

In this thesis the SRT system has been studied as one entity. The SRT system was examined and set up in order to make it operational for future observations. The fundamentals of radio astronomy and the SRT system were explained. In radio astronomy there are many different types of systems and implementations, yet all of these systems have common qualities. The description of these common qualities was considered to form a basis for all who are interested in working with the SRT system, or with radio astronomy in general.

The most sensitive parts of the SRT system were probed and weaknesses were found. In the SRT's outside surroundings, the weather conditions and the normal physical wear of the parts and joints will be a negative influence to the system in the future, unless these issues are addressed and attended to. Further insulation into the wiring and into the box that encloses the receiver, LNA and band-pass filter will make it more resil-

ient against weather, moisture, wear out failure and corrosion. These findings will help resolve the possible future inconveniences, when the SRT will be operational every day of the year.

The University staff was also given a demonstration of how the system works and what was done during this study. This left them better equipped to use the SRT to its maximum capacity and to make many interesting observations in the future.

## References

[1] Assembly Instructions for CASSI Mount

[2] Bevelacqua, Peter Joseph. Antenna Efficiency and Antenna Gain. Internet document. <http://www.antenna-theory.com/basics/gain.php>. Accessed 20 February 2014.

[3] CA World Wifi. 2408U-PRO, 2.4 Ghz antenna, 8 Dbi gain. Internet document. <http://www.caworldwifi.com/2408U-PRO-omni-wifi-antenna.html>. Accessed 20 February 2014.

[4] EM Talk. Microstrip Line Calculator. Internet document. <http://www.emtalk.com/mscalc.php?er=fr4&h=1&h_units_list=hmm&f=1.4&Zo=NAN&EL=NAN&Operation=Synthesize&Wa=-9.90012466017&W_units_list=Wmm&La=220&L_units_list=Lmm>. Accessed 20 February 2014.

[5] Giancoli, Douglas C. 1998. Physics. 5th ed. Upper Saddle River: Prentice-Hall, Inc.

[6] Graham-Smith, F. 1960. Radio Astronomy. London: The Whitefriars Press Ltd.

[7] Kraus, John D.1966, Radio Astronomy. New York: McGraw-Hill.

[8] Lehto, Arto. 2006. Radioaaltojen maailma. Helsinki: Otatieto.

[9] National Radio Astronomy Observatory. Welcome to the Very Large Array! Internet document. <http://www.vla.nrao.edu/>. Accessed 20 February 2014.

[10] NEROC HAYSTACK OBSERVATORY SRT MANUAL

[11] Ott, Henry W. 1988. Noise Reduction Techiques in Electronic System. New York: John Wiley & Sons, Inc.

[12] Razavi, Behzad. 1998. RF Microelectronics. Upper Saddle River: Prentice-Hall, Inc.

[13] Rohlfs, K., Wilson, T.L. 2004. Tools of Radio Astronomy. 4th ed. Berlin: Springer-Verlag.

[14] Räisänen, A., Lehto, A. 2011. Radiotekniikan perusteet. Helsinki: Otatieto.

[15] Steinberg, J.L., Lequeux, J. 1963. Radio Astronomy. New York: McGraw-Hill.

[16] URSA. Maailmankaikkeus 2013-2014

[17] U.S. Naval Observatory (USNO). Astrographic Catalogue History and Zone Information. <http://ad.usno.navy.mil/proj/AC/hist.html>. Accessed 20 February 2014.

**Antenna Assembly Instructions**

# Antenna Assembly Instructions

Required Tools:

1 - 1/2" & 7/16" Open End Wrenches
1 - 16" Adjustable Wrench
1 - Steel Tape Measure
1 - 7/16" Socket and Ratchet
1 - 3/4" Open End Wrench

**Step 1.** It is necessary to assemble the reflector on a flat surface to ensure proper alignment of the sections. It is a good idea to protect the surface finish by placing cardboard, etc., under the edge of the reflector. Begin by assembling any two quadrants with the 1/4"-20 x 2" bolts through the three outermost pre-drilled and the innermost hole of the sections on the Quad 7.5' antenna. Use 1/4" flat washers on both sides of the rib, at each assembly point. *Finger Tighten Only At This Time*.



Figure 1. Place all four quadrants on a flat surface prior to assembly.



Figure 2. Only install the outer 2 bolts (7.5-foot dish) or outer 3 bolts (10-foot dish)

**Step 2.** Repeat step 1 by assembling the remaining two quadrants. Now you have two halves. The two halves can be bolted together remembering to *Finger Tighten Only* at this time. Now make sure all the quadrants are properly joined and flush at each assembly point. *THIS IS VERY IMPORTANT TO ASSURE THE CURVE OF THE REFLECTOR IS MAINTAINED AND SUPPORTED CORRECTLY.* Wrench tighten all bolts at this time.



Figure 3. Assembly of the parabolic dish as described in the instructions above.

**Step 3.** You may stand the assembled reflector on edge for easy access to the center. Attach the center hub plates to the antenna by inserting four 5/16" x 2" carriage bolts through the front plate, between the ribs, and through the rear plate on the backside of the reflector. Be sure to use 5/16" washers on the rear hub plate. *SECURELY TIGHTEN THE CARRIAGE BOLTS WITH A WRENCH.*

**Step 4.** This step involves attaching the quad feed supports. Carefully lay the antenna down on its back so the reflective surface is facing up.

Holes are drilled in each reflector section to accommodate the Quad Feed Support. Attach the end of the feed support rod with the round hole to the outside perimeter of the antenna with 1/4"-20 x 1-1/2" bolts. The feed supports attach through holes in the face of the reflector. The slotted end of the feed support rod attaches to the feed horn with 1/4"-20 x 3/4" bolts. *THE FEED SUPPORTS SHOULD BE POSITIONED EQUALLY TO PROPERLY CENTER THE FEED HORN.*
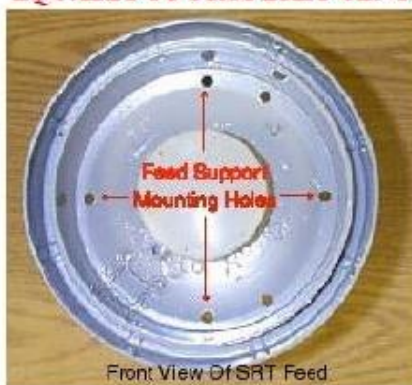


Figure 4. SRT feed horn

When installing the feed supports place the head of the 1/4-20 bolt inside the feed. This creates a lower profile than placing the nut and lock washer inside the feed.

Secure the slotted ends of the feed supports to the feed horn.
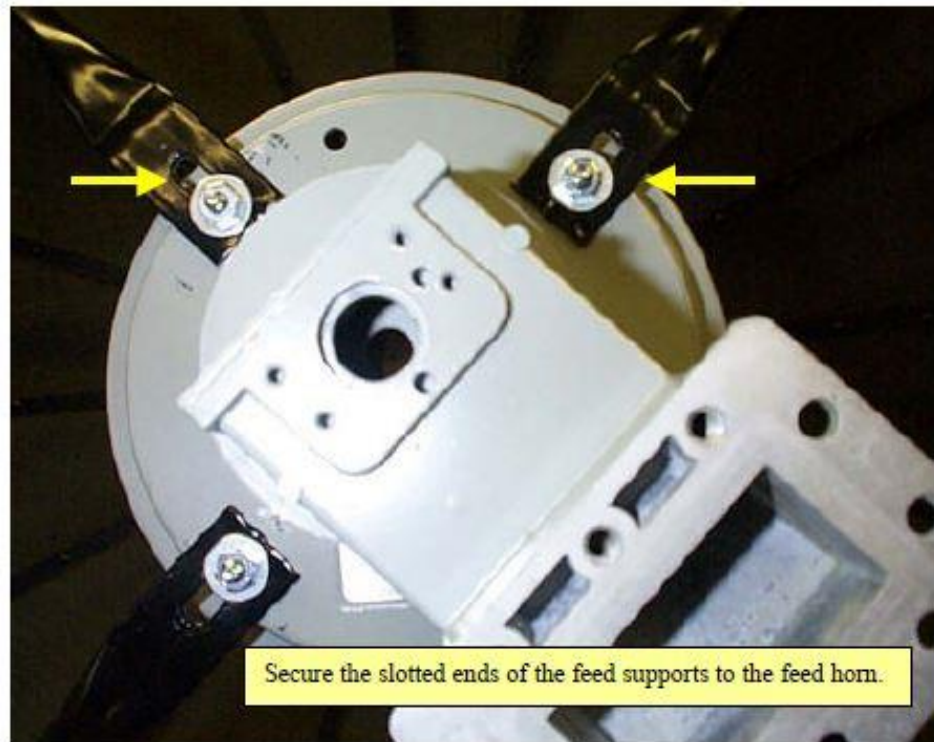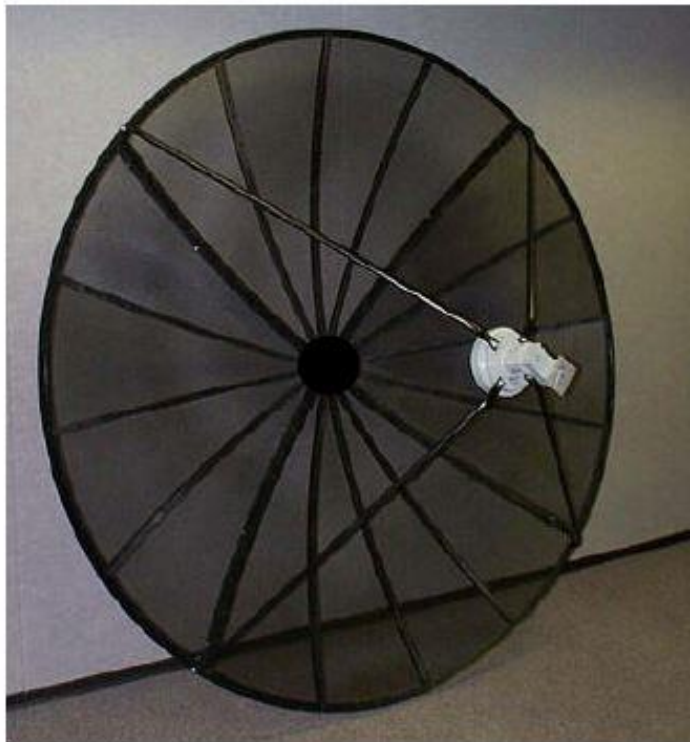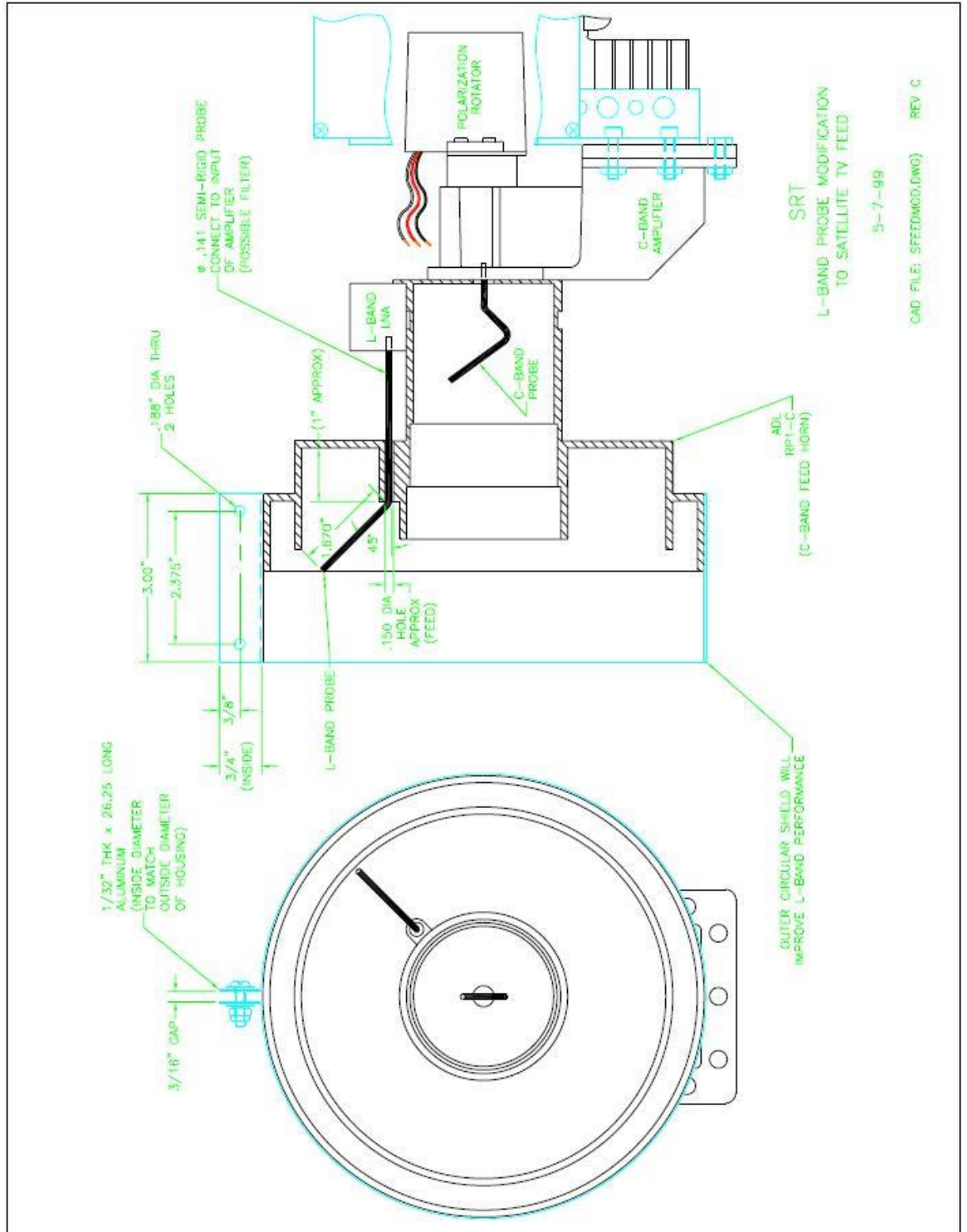
Figure 5. Properly installed feed horn.



Figure 6. Antenna assembly

The dish is now ready to be mounted on the two-axis mount using the mounting ring provided.

**Antenna Feed**



SRT
L-BAND PROBE MODIFICATION
TO SATELLITE TV FEED

5-7-99

CAD FILE: SFEEDMOD.DWG)    REV C

# Cassi Mount Assembly Instructions

## Assembly Instructions for
## CASSI Mount

This is the supplemental assembly instructions for the AZ/EL CASSI mount supplied with the Small Radio Telescope kit. The mount comes partially assembled and wired but requires some user assembly. Documentation describing the rest of the installation of the SRT can be found on the website. A special complied version of the software has been produced with appropriate defaults for the new mount.



The CASSI mount comes on a pallet containing the main motor gearbox assembly, a screw jack linear actuator for the elevation axis and left and right dish ring riser arms located in a separate box on the pallet. The main gearbox weighs over 120 lbs and needs 2-3 people to lift onto the mast. The mast needs to be made of 3 inch schedule 40 steel pipe and extend at least four feet above the ground for the 7.5 foot dish. See separate documentation for constructing the pier and mast assembly.

The flat end (door) of the gear box nominally points north but the exact orientation depends on the setting of the internal limit switch and the Az software limit set up in the SRT.CAT file located in the directory containing the java code for the SRT system. The software and controller are not needed for initial assembly of the mount but will be needed to attach the feed horn and receiver.

Once the motor gearbox is on the mast locate and mount the elevation linear actuator and attach it to the lifter arm extending up from the cradle which forms the elevation axis. The linear actuator is preconfigured and should not be activated or have its end rod rotated by hand as this sets one of the limit switches and can damage the unit if done incorrectly (see manufacturer instructions in the box). The gearmotor at the end of the actuator should point up when attached to the lifter arm.



Locate the two riser arms shipped in the actuator box located on the pallet. The "T" shaped arm should be mounted on the same end of the cradle where the lifter arm is located. Attach the arms by removing the two ¾ inch nuts and sandwich the arms between the two washers. A small amount of grease can be applied to aid in movement and prevent rust. Only hand tighten the nuts for now. The second nuts are used as locking nuts to prevent loosening.



Locate the dish mounting ring which is part of the dish shipment and attach it to the riser arms. The ring should attach in only one orientation. Once the ring is attached to the riser arms you can tighten the elevation nuts short of binding the movement of the ring. The end rod of the elevation linear actuator can now be attached to a small tab on the mounting ring. The ring should be in a horizontal position (dish looking at zenith). The sections of the dish should now be assembled and the completed dish lifted up and positioned on the mounting ring. Attach using bolts provided.



There are two versions of the mount which differ in how the 9 conductor and elevation actuator cables are routed to the screw down blocks inside the gearbox. See the appropriate figure. Locate the 9 conductor cable which connects the
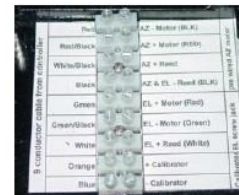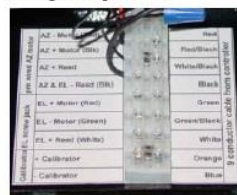
controller to the antenna mount. Remove about 3 inches of the outer insulating jacket and strip and solder the ends of each of the conductors about 3/8 inch. Route the 9 conductor cable up through the bottom of the mount and attach the ends to the screw down block according to the wiring diagram.

The Az motor and reed sensor should already be connected to their associated side of the screw down block. Strip about 2 inches of the outer jacket of the linear actuator cable and strip about 3/8 inch from each of the conductors and solder all but the black conductor. Route the cable from the actuator through the right (or left) hole in the bottom of the mount and attach according to the wiring diagram. The black conductor for the cable must share a connection with the Az reed switch by including it in the wire nut connection already in place.
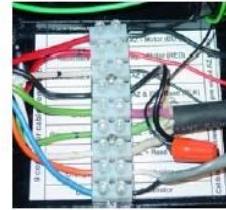


Finally, route the 2 conductor cable for the calibrator through the hole on the bottom of the mount and attach according to the wiring diagram. When routing the calibrator cable from the mount to the calibrator take care that it will not get hung up as the system rotates. I use electrical tape to attach it to the lifter arm exactly like the cable from the linear actuator before going to the actual calibrator.

To gain access to the dish and attach the receiver to the support legs you will need to install the software and connect the 9 conductor cable to the controller. The SRT.CAT file needs to be modified by commenting out the keyword "SIMULATE ANTENNA" by inserting a asterisk (*) in the first column of that line. When the software is started up and the controller is on the dish should go to its zero point as defined in the SRT.CAT file which is due north at nearly zero degrees elevation. The orientation of the mount and the elevation of the dish when at these limits should agree with the first numbers associated with the AZLIMITS and ELLIMITS keywords.
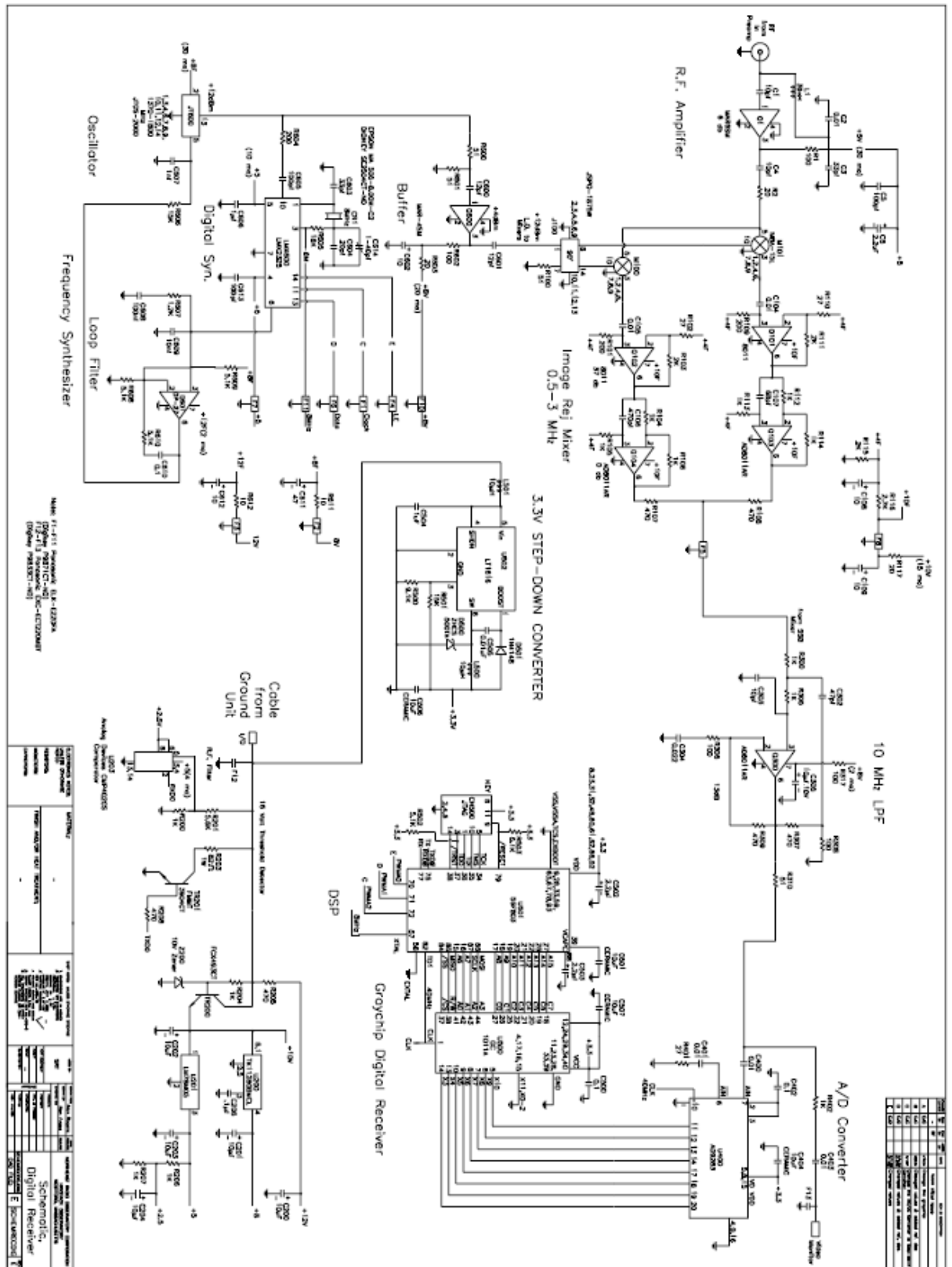
**SRT Receiver Block Diagram**
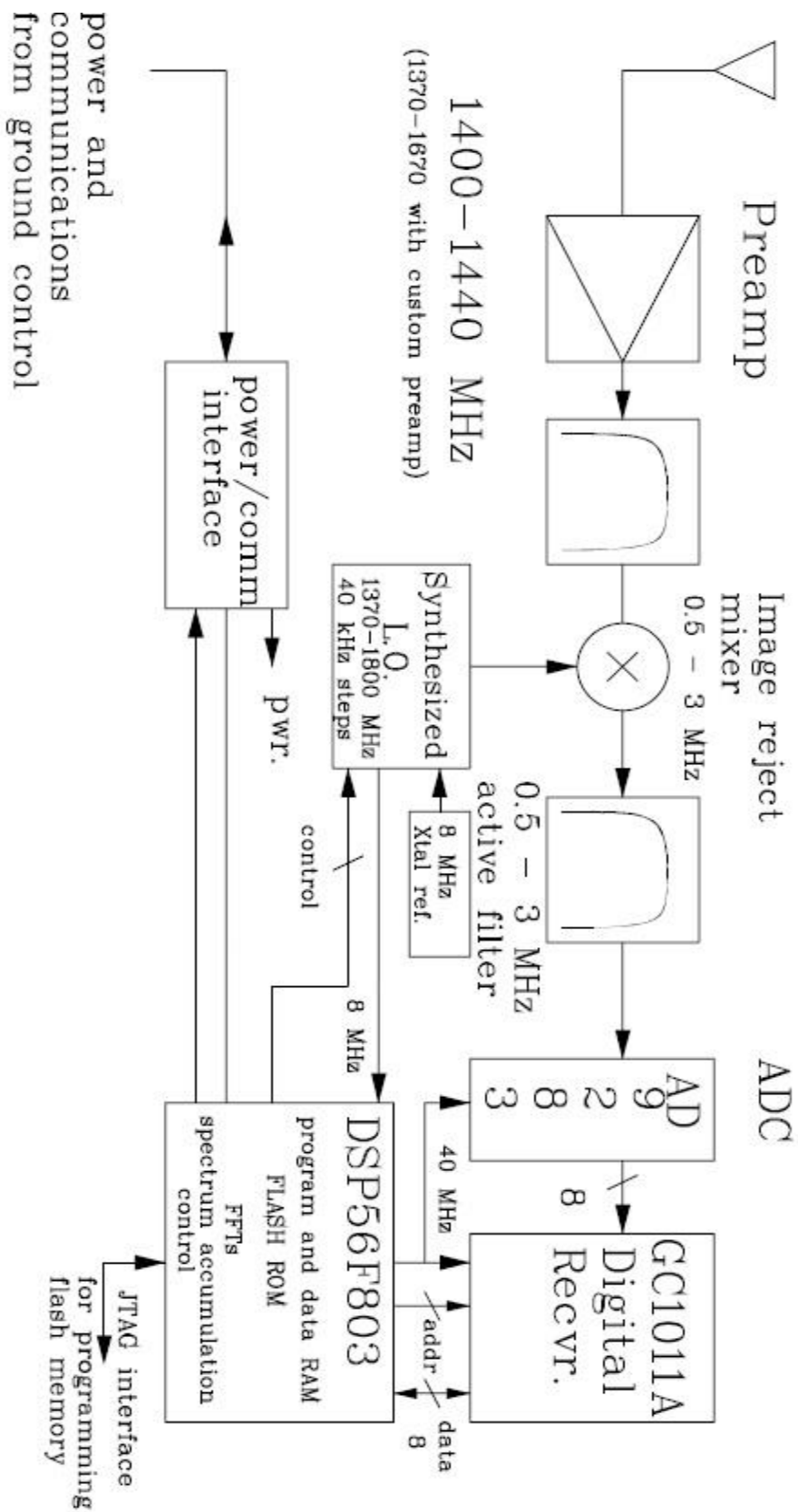


Digital Receiver for SRT

# SRT Receiver Schematics



Schematic, Digital Receiver

## SRT LNA Schematics
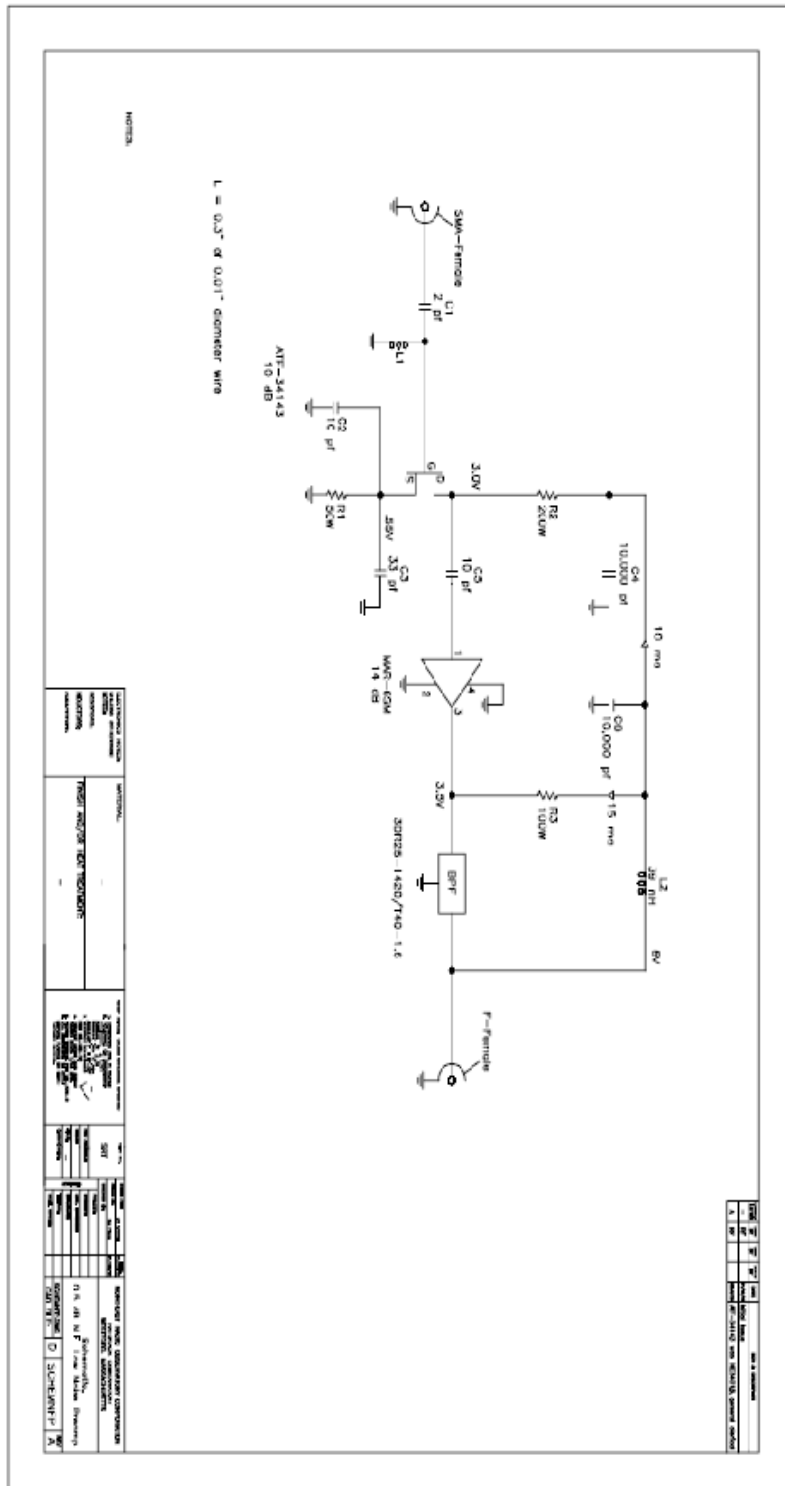
## SRT Ground Controller Schematics
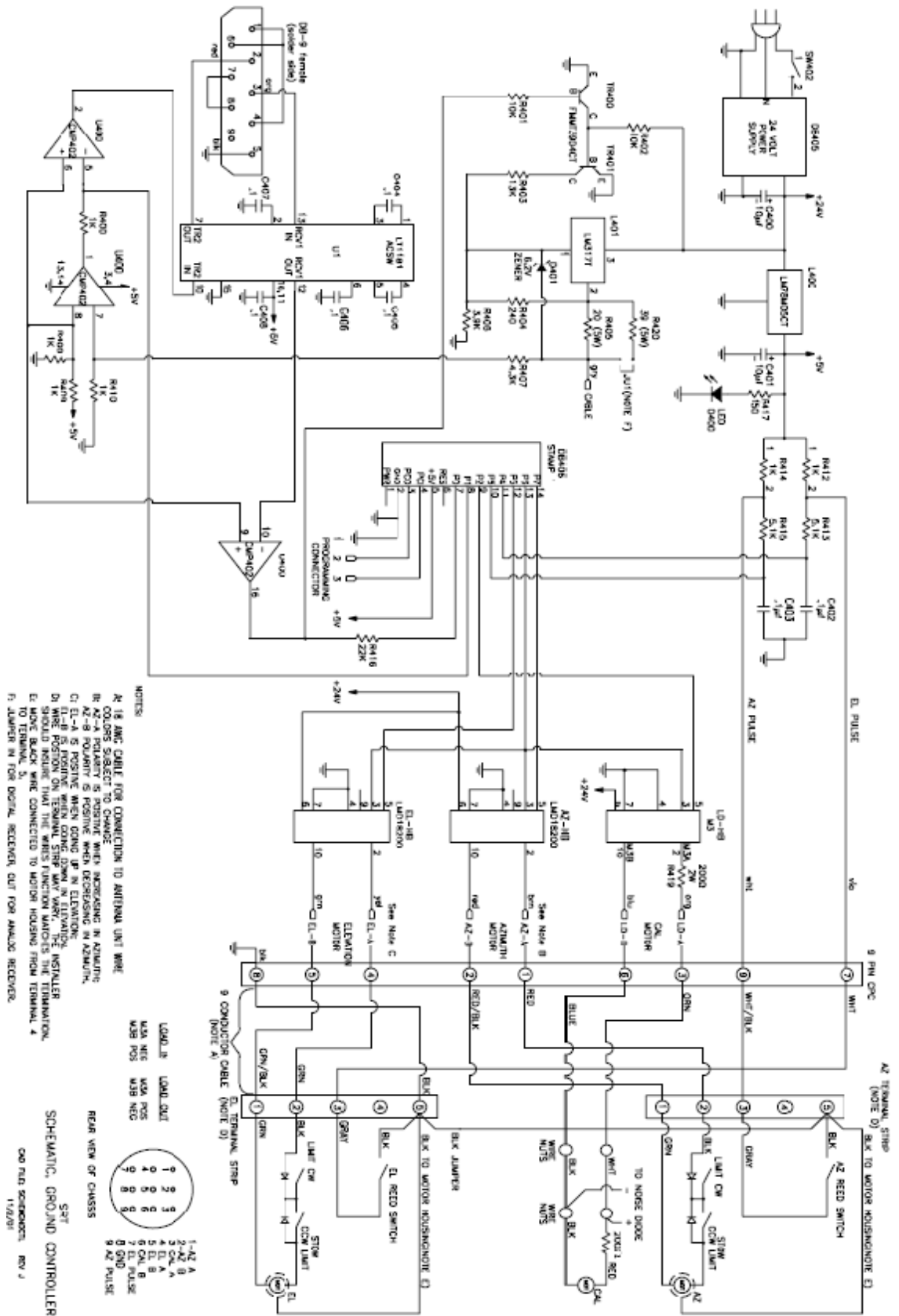
**SRT Receiver Characteristics**

*Digital Receiver*

| | |
|---|---|
| **L.O. Frequency range** | 1370-1800 MHz |
| **L.O. Tuning steps** | 40 kHz |
| **L.O. Settle time** | <5 ms |
| **Rejection of LSB image** | >20 dB |
| **Bandwidth/Resolution Modes** | 1200/8 kHz* |
| ***(Currently supported in ver 1.0 firmware)*** | 500/8 kHz |
| - | 250/4 kHz |
| - | 125/2 kHz |
| **I.F. Center** | 800 kHz |
| **6 dB I.F. range** | 0.5-3 MHz |
| **Preamp frequency range** | 1400-1440 MHz |
| **Typical system temperature** | 150K |
| **Typical L.O. leakage out of preamp** | -105dBm |
| **Preamp input for dB compression from out of band signals** | -24 dBm |
| **Preamp input for intermodulation interference** | -30 dBm |
| **Control** | RS-232 2400 baud |

 * The 1200 kHz wideband is synthesized using 3 500 kHz bands stitched together from a frequency scan.

*Digital Receiver Board*
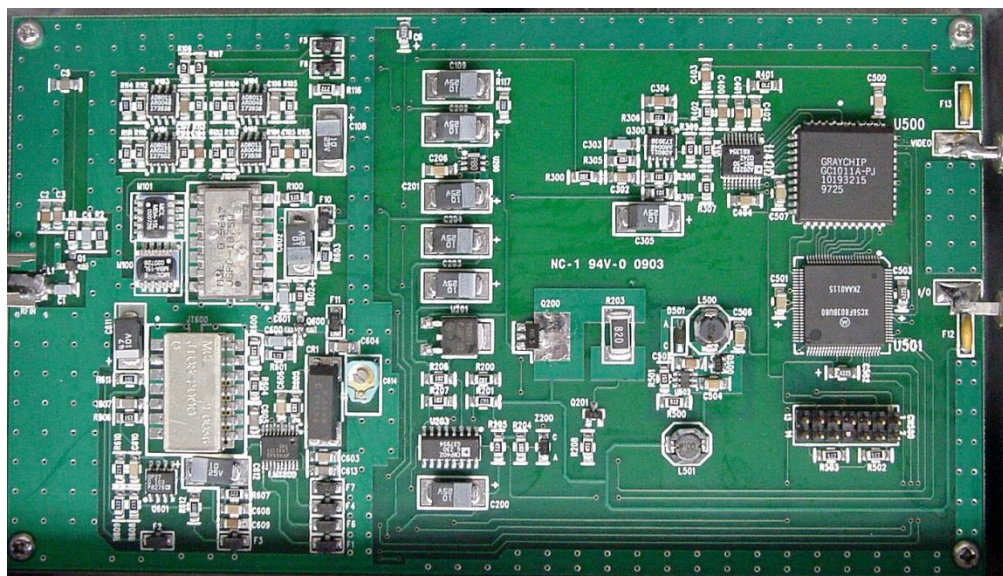
**ATF-34143 HEMT Datasheet**

## ATF-34143
## Low Noise Pseudomorphic HEMT
## in a Surface Mount Plastic Package

## Data Sheet

**Avago**
TECHNOLOGIES

### Description

Avago's ATF-34143 is a high dynamic range, low noise PHEMT housed in a 4-lead SC-70 (SOT-343) surface mount plastic package.

Based on its featured performance, ATF-34143 is ideal for the first stage of base station LNA due to the excellent combination of low noise figure and high linearity[1]. The device is also suitable for applications in Wireless LAN, WLL/RLL, MMDS, and other systems requiring super low noise figure with good intercept in the 450 MHz to 10 GHz frequency range.

**Note:**
1. From the same PHEMT FET family, the larger geometry ATF-33143 may also be considered either for the higher linearity performance or easier circuit design for stability in the lower frequency bands (800–900 MHz).

### Surface Mount Package - SOT-343
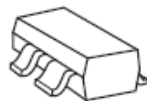
### Pin Connections and Package Marking

DRAIN — — SOURCE

SOURCE — 4Px — GATE
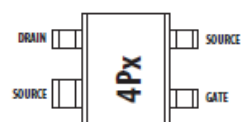
**Note:** Top View. Package marking provides orientation and identification.

"4P" = Device code
"x" = Date code character. A new character is assigned for each month, year.

### Features

- Lead-free Option Available
- Low Noise Figure
- Excellent Uniformity in Product Specifications
- 800 micron Gate Width
- Low Cost Surface Mount  Small Plastic Package SOT-343 (4 lead SC-70)
- Tape-and-Reel Packaging Option Available

### Specifications

**1.9 GHz; 4V, 60 mA (Typ.)**

- 0.5 dB Noise Figure
- 17.5 dB Associated Gain
- 20 dBm Output Power at 1 dB Gain Compression
- 31.5 dBm Output 3rd Order Intercept

### Applications

- Tower Mounted Amplifier and Low Noise Amplifier for GSM/TDMA/CDMA Base Stations
- LNA for Wireless LAN, WLL/RLL and MMDS Applications
- General Purpose Discrete PHEMT for other Ultra Low Noise Applications

**Attention: Observe precautions for handling electrostatic sensitive devices.**
ESD Machine Model (Class A)
ESD Human Body Model (Class 0)
Refer to Avago Application Note A004R:
*Electrostatic Discharge Damage and Control.*

## ATF-34143 Absolute Maximum Ratings[1]

| Symbol | Parameter | Units | Absolute Maximum |
|--------|-----------|-------|------------------|
| $V_{DS}$ | Drain - Source Voltage[2] | V | 5.5 |
| $V_{GS}$ | Gate - Source Voltage[2] | V | -5 |
| $V_{GD}$ | Gate Drain Voltage[2] | V | -5 |
| $I_D$ | Drain Current[2] | mA | $I_{dss}$[3] |
| $P_{diss}$ | Total Power Dissipation[4] | mW | 725 |
| $P_{in\ max}$ | RF Input Power | dBm | 17 |
| $T_{CH}$ | Channel Temperature | °C | 160 |
| $T_{STG}$ | Storage Temperature | °C | -65 to 160 |
| $\theta_{jc}$ | Thermal Resistance[5] | °C/W | 165 |

**Notes:**
1. Operation of this device above any one of these parameters may cause permanent damage.
2. Assumes DC quiescent conditions.
3. $V_{GS}$ = 0 volts.
4. Source lead temperature is 25°C. Derate 6 mW/°C for $T_L$ > 40°C.
5. Thermal resistance measured using 150°C Liquid Crystal Measurement method.
6. Under large signal conditions, $V_{GS}$ may swing positive and the drain current may exceed $I_{dss}$. These conditions are acceptable as long as the maximum $P_{diss}$ and $P_{in\ max}$ ratings are not exceeded.

## Product Consistency Distribution Charts [7]
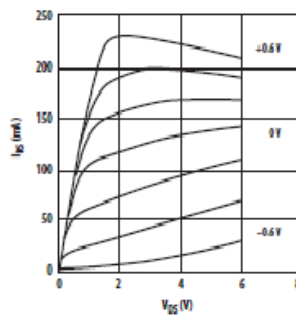


Figure 1. Typical/Pulsed I-V Curves[6].
($V_{GS}$ = -0.2 V per step)
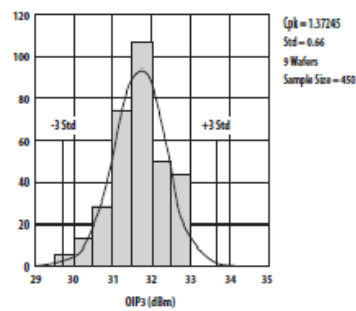


Figure 2. OIP3 @ 2 GHz, 4†V, 60 mA.
LSL=29.0, Nominal=31.8, USL=35.0
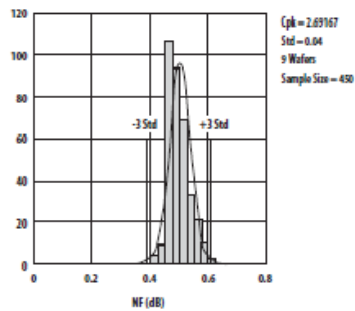


Figure 3. NF @ 2 GHz, 4†V, 60 mA.
LSL=0.1, Nominal=0.47, USL=0.8



Figure 4. Gain @ 2 GHz, 4†V, 60 mA.
LSL=16.0, Nominal=17.5, USL=19.0

Notes:
7. Distribution data sample size is 450 samples taken from 9 different wafers. Future wafers allocated to this product may have nominal values anywhere within the upper and lower spec limits.
8. Measurements made on production test board. This circuit represents a trade-off between an optimal noise match and a realizeable match based on production test requirements. Circuit losses have been de-embedded from actual measurements.

## ATF-34143 Electrical Specifications

$T_A = 25°C$, RF parameters measured in a test circuit for a typical device

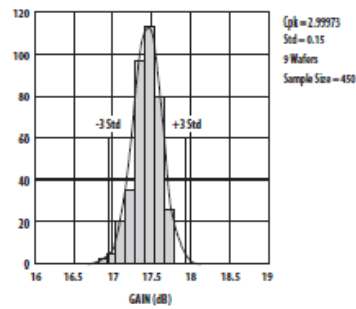| Symbol | Parameters and Test Conditions | | | Units | Min. | Typ.[2] | Max. |
|---|---|---|---|---|---|---|---|
| $I_{dss}$[1] | Saturated Drain Current | | $V_{DS} = 1.5 V, V_{GS} = 0 V$ | mA | 90 | 118 | 145 |
| $V_P$[1] | Pinchoff Voltage | | $V_{DS} = 1.5 V, I_{DS} = 10\%$ of $I_{dss}$ | V | -0.65 | -0.5 | -0.35 |
| $I_d$ | Quiescent Bias Current | | $V_{GS} = -0.34 V, V_{DS} = 4 V$ | mA | — | 60 | — |
| $g_m$[1] | Transconductance | | $V_{DS} = 1.5 V, g_m = I_{dss}/V_P$ | mmho | 180 | 230 | — |
| $I_{GDO}$ | Gate to Drain Leakage Current | | $V_{GD} = 5 V$ | µA | | | 500 |
| $I_{gss}$ | Gate Leakage Current | | $V_{GD} = V_{GS} = -4 V$ | µA | — | 30 | 300 |
| NF | Noise Figure | f = 2 GHz | $V_{DS} = 4 V, I_{DS} = 60 mA$ | dB | | 0.5 | 0.8 |
| | | | $V_{DS} = 4 V, I_{DS} = 30 mA$ | | | 0.5 | |
| | | f = 900 MHz | $V_{DS} = 4 V, I_{DS} = 60 mA$ | dB | | 0.4 | |
| $G_a$ | Associated Gain | f = 2 GHz | $V_{DS} = 4 V, I_{DS} = 60 mA$ | dB | 16 | 17.5 | 19 |
| | | | $V_{DS} = 4 V, I_{DS} = 30 mA$ | | | 17 | |
| | | f = 900 MHz | $V_{DS} = 4 V, I_{DS} = 60 mA$ | dB | | 21.5 | |
| OIP3 | Output 3rd Order Intercept Point[3] | f = 2 GHz +5 dBm $P_{out}$/Tone | $V_{DS} = 4 V, I_{DS} = 60 mA$ | dBm | 29 | 31.5 | |
| | | | $V_{DS} = 4 V, I_{DS} = 30 mA$ | | | 30 | |
| | | f = 900 MHz +5 dBm $P_{out}$/Tone | $V_{DS} = 4 V, I_{DS} = 60 mA$ | dBm | | 31 | |
| $P_{1dB}$ | 1 dB Compressed Intercept Point[3] | f = 2 GHz | $V_{DS} = 4 V, I_{DS} = 60 mA$ | dBm | | 20 | |
| | | | $V_{DS} = 4 V, I_{DS} = 30 mA$ | | | 19 | |
| | | f = 900 MHz | $V_{DS} = 4 V, I_{DS} = 60 mA$ | dBm | | 18.5 | |

Notes:
1. Guaranteed at wafer probe level
2. Typical value determined from a sample size of 450 parts from 9 wafers.
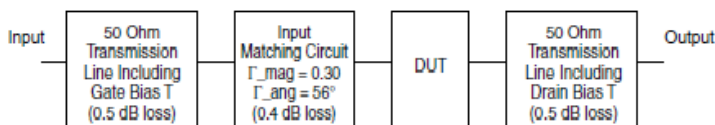3. Using production test board.



Figure 5. Block diagram of 2 GHz production test board used for Noise Figure, Associated Gain, P1dB, and OIP3 measurements. This circuit represents a trade-off between an optimal noise match and associated impedance matching circuit losses. Circuit losses have been de-embedded from actual measurements.

## ATF-34143 Typical Performance Curves
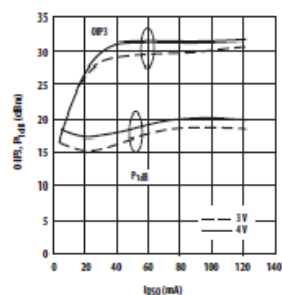


Figure 6. OIP3 and $P_{1dB}$ vs. $I_{DS}$ and $V_{DS}$ Tuned for NF @ 4 V, 60 mA at 2 GHz. [1,2]
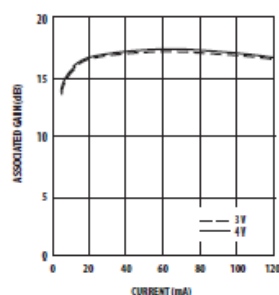


Figure 7. Associated Gain vs. Current ($I_d$) and Voltage ($V_D$) at 2 GHz. [1,2]



Figure 8. Noise Figure vs. Current ($I_d$) and Voltage ($V_{DS}$) at 2 GHz. [1,2]
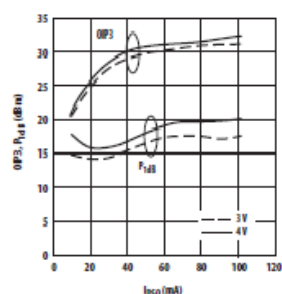


Figure 9. OIP3 and $P_{1dB}$ vs. $I_{DS}$ and $V_{DS}$ Tuned for NF @ 4 V, 60 mA at 900 MHz. [1,2]
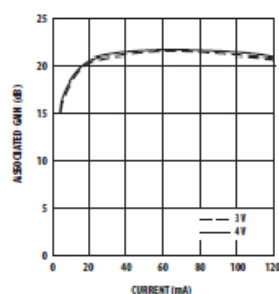


Figure 10. Associated Gain vs. Current ($I_d$) and Voltage ($V_D$) at 900 MHz. [1,2]



Figure 11. Noise Figure vs. Current ($I_d$) and Voltage ($V_{DS}$) at 900 MHz. [1,2]
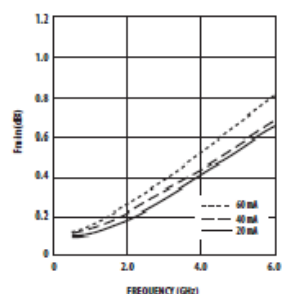


Figure 12. Fmin vs. Frequency and Current at 4 V.
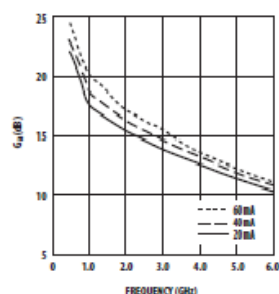


Figure 13. Associated Gain vs. Frequency and Current at 4 V.

**Notes:**
1. Measurements made on a fixed toned production test board that was tuned for optimal gain match with reasonable noise figure at 4V, 60 mA bias. This circuit represents a trade-off between optimal noise match, maximum gain match, and a realizable match based on production test board requirements. Circuit losses have been de-embedded from actual measurements.
2. $P_{1dB}$ measurements are performed with passive biasing. Quiescent drain current, $I_{DSQ}$, is set with zero RF drive applied. As $P_{1dB}$ is approached, the drain current may increase or decrease depending on frequency and dc bias point. At lower values of $I_{DSQ}$ the device is running closer to class B as power output approaches $P_{1dB}$. This results in higher PAE (power added efficiency) when compared to a device that is driven by a constant current source as is typically done with active biasing. As an example, at a $V_{DS} = 4$ V and $I_{DSQ} = 10$ mA, $I_d$ increases to 62 mA as a $P_{1dB}$ of +19 dBm is approached.

4

## ATF-34143 Typical Performance Curves, continued
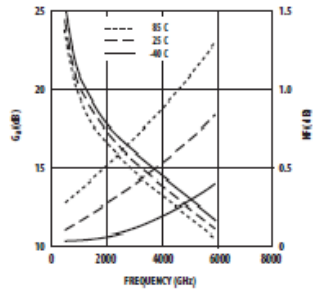


Figure 14. Fmin and $G_a$ vs. Frequency and Temperature at $V_{DS} = 4$ V, $I_{DS} = 60$ mA.
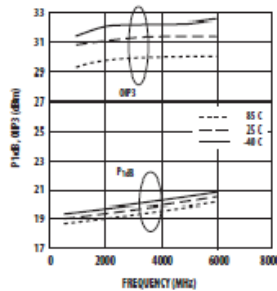


Figure 15. $P_{1dB}$, IP3 vs. Frequency and Temperature at $V_{DS} = 4$ V, $I_{DS} = 60$ mA. [1]
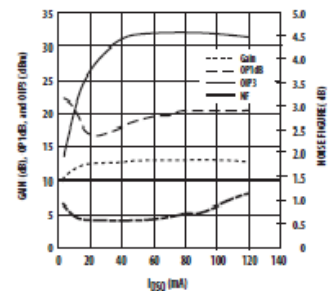


Figure 16. NF, Gain, OP1dB and OIP3 vs. $I_{DS}$ at 4 V and 3.9 GHz Tuned for Noise Figure. [1]
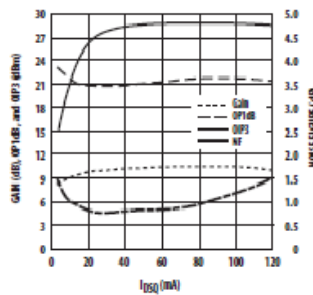


Figure 17. NF, Gain, OP1dB and OIP3 vs. $I_{DS}$ at 4 V and 5.8 GHz Tuned for Noise Figure. [1]
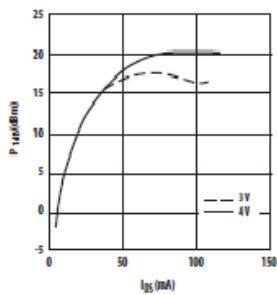


Figure 18. $P_{1dB}$ vs. $I_{DS}$ Active Bias Tuned for NF @ 4 V, 60 mA at 2 GHz.
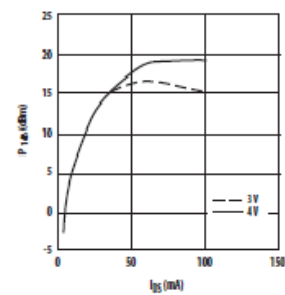


Figure 19. $P_{1dB}$ vs. $I_{DS}$ Active Bias Tuned for min NF @ 4V, 60 mA at 900 MHz.

Note:

1. $P_{1dB}$ measurements are performed with passive biasing. Quiescent drain current, $I_{DSQ}$, is set with zero RF drive applied. As $P_{1dB}$ is approached, the drain current may increase or decrease depending on frequency and dc bias point. At lower values of $I_{DSQ}$ the device is running closer to class B as power output approaches $P_{1dB}$. This results in higher PAE (power added efficiency) when compared to a device that is driven by a constant current source as is typically done with active biasing. As an example, at a $V_{DS} = 4$ V and $I_{DSQ} = 10$ mA, $I_d$ increases to 62 mA as a $P_{1dB}$ of +19 dBm is approached.

**ATF-34143 Power Parameters tuned for Power, $V_{DS}$ = 4 V, $I_{DSQ}$ = 120 mA**

| Freq (GHz) | $P_{1dB}$ (dBm) | $I_d$ (mA) | $G_{1dB}$ (dB) | $PAE_{1dB}$ (%) | $P_{1dBm}$ (dBm) | $I_d$ (mA) | $PAE_{dB}$ (%) | Gamma Out_mag (Mag) | Gamma Out_ang [Degrees] |
|---|---|---|---|---|---|---|---|---|---|
| 0.9 | 20.9 | 114 | 25.7 | 27 | 22.8 | 108 | 44 | 0.34 | 136 |
| 1.5 | 21.7 | 115 | 21.9 | 32 | 23.1 | 95 | 53 | 0.31 | 152 |
| 1.8 | 21.3 | 111 | 20.5 | 30 | 23.0 | 105 | 47 | 0.30 | 164 |
| 2 | 22.0 | 106 | 19.5 | 37 | 23.7 | 115 | 50 | 0.28 | 171 |
| 4 | 22.7 | 110 | 12.7 | 40 | 23.6 | 111 | 47 | 0.26 | -135 |
| 6 | 23.3 | 115 | 9.2 | 41 | 24.2 | 121 | 44 | 0.24 | -66 |

**ATF-34143 Power Parameters tuned for Power, $V_{DS}$ = 4 V, $I_{DSQ}$ = 60 mA**

| Freq (GHz) | $P_{1dB}$ (dBm) | $I_d$ (mA) | $G_{1dB}$ (dB) | $PAE_{1dB}$ (%) | $P_{1dBm}$ (dBm) | $I_d$ (mA) | $PAE_{dB}$ (%) | Gamma Out_mag (Mag) | Gamma Out_ang [Degrees] |
|---|---|---|---|---|---|---|---|---|---|
| 0.9 | 18.2 | 75 | 27.5 | 22 | 20.5 | 78 | 36 | 0.48 | 102 |
| 1.5 | 18.7 | 58 | 24.5 | 32 | 20.8 | 59 | 51 | 0.45 | 117 |
| 1.8 | 18.8 | 57 | 23.0 | 33 | 21.1 | 71 | 45 | 0.42 | 126 |
| 2 | 18.8 | 59 | 22.2 | 32 | 21.9 | 81 | 47 | 0.40 | 131 |
| 4 | 20.2 | 66 | 13.9 | 38 | 22.0 | 77 | 48 | 0.25 | -162 |
| 6 | 21.2 | 79 | 9.9 | 37 | 23.5 | 102 | 46 | 0.18 | -77 |
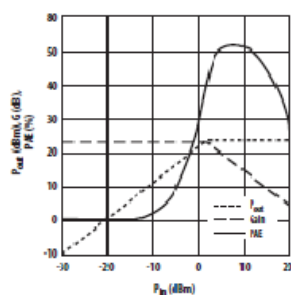


Figure 20. Swept Power Tuned for Power at 2 GHz, $V_{DS}$= 4V, $I_{DSQ}$=120 mA.
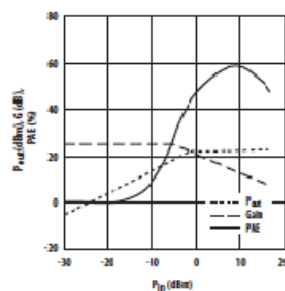
Figure 21. Swept Power Tuned for Power at 2 GHz, $V_{DS}$ = 4 V, $I_{DSQ}$ = 60 mA.

**Notes:**

1. $P_{1dB}$ measurements are performed with passive biasing. Quiescent drain current, $I_{DSQ}$, is set with zero RF drive applied. As $P_{1dB}$ is approached, the drain current may increase or decrease depending on frequency and dc bias point. At lower values of $I_{DSQ}$ the device is running closer to class B as power output approaches $P_{1dB}$. This results in higher PAE (power added efficiency) when compared to a device that is driven by a constant current source as is typically done with active biasing. As an example, at a $V_{DS}$ = 4 V and $I_{DSQ}$ = 10 mA, $I_d$ increases to 62 mA as a $P_{1dB}$ of +19 dBm is approached.
2. PAE(%) = ((Pout – Pin)/Pdc) x 100
3. Gamma out is the reflection coefficient of the matching circuit presented to the output of the device.

### ATF-34143 Typical Scattering Parameters, $V_{DS} = 3\,V$, $I_{DS} = 20\,mA$

| Freq. GHz | $S_{11}$ Mag. | Ang. | dB | $S_{21}$ Mag. | Ang. | dB | $S_{12}$ Mag. | Ang. | $S_{22}$ Mag. | Ang. | MSG/MAG dB |
|---|---|---|---|---|---|---|---|---|---|---|---|
| 0.5 | 0.96 | -37 | 20.07 | 10.079 | 153 | -29.12 | 0.035 | 68 | 0.40 | -35 | 24.59 |
| 0.8 | 0.91 | -60 | 19.68 | 9.642 | 137 | -26.02 | 0.050 | 56 | 0.34 | -56 | 22.85 |
| 1.0 | 0.87 | -76 | 18.96 | 8.867 | 126 | -24.29 | 0.061 | 48 | 0.32 | -71 | 21.62 |
| 1.5 | 0.81 | -104 | 17.43 | 7.443 | 106 | -22.27 | 0.077 | 34 | 0.29 | -98 | 19.85 |
| 1.8 | 0.78 | -115 | 16.70 | 6.843 | 98 | -21.62 | 0.083 | 28 | 0.28 | -110 | 19.16 |
| 2.0 | 0.75 | -126 | 16.00 | 6.306 | 90 | -21.11 | 0.088 | 23 | 0.26 | -120 | 18.55 |
| 2.5 | 0.72 | -145 | 14.71 | 5.438 | 75 | -20.45 | 0.095 | 15 | 0.25 | -140 | 17.58 |
| 3.0 | 0.69 | -162 | 13.56 | 4.762 | 62 | -19.83 | 0.102 | 7 | 0.23 | -156 | 16.69 |
| 4.0 | 0.65 | 166 | 11.61 | 3.806 | 38 | -19.09 | 0.111 | -8 | 0.22 | 174 | 15.35 |
| 5.0 | 0.64 | 139 | 10.01 | 3.165 | 16 | -18.49 | 0.119 | -21 | 0.22 | 146 | 14.25 |
| 6.0 | 0.65 | 114 | 8.65 | 2.706 | -5 | -18.06 | 0.125 | -35 | 0.23 | 118 | 13.35 |
| 7.0 | 0.66 | 89 | 7.33 | 2.326 | -27 | -17.79 | 0.129 | -49 | 0.25 | 91 | 10.91 |
| 8.0 | 0.69 | 67 | 6.09 | 2.017 | -47 | -17.52 | 0.133 | -62 | 0.29 | 67 | 9.71 |
| 9.0 | 0.72 | 48 | 4.90 | 1.758 | -66 | -17.39 | 0.135 | -75 | 0.34 | 46 | 8.79 |
| 10.0 | 0.75 | 30 | 3.91 | 1.568 | -86 | -17.08 | 0.140 | -88 | 0.39 | 28 | 8.31 |
| 11.0 | 0.77 | 10 | 2.88 | 1.393 | -105 | -16.95 | 0.142 | -103 | 0.43 | 10 | 7.56 |
| 12.0 | 0.80 | -10 | 1.74 | 1.222 | -126 | -16.95 | 0.142 | -118 | 0.47 | -10 | 6.83 |
| 13.0 | 0.83 | -29 | 0.38 | 1.045 | -145 | -17.39 | 0.135 | -133 | 0.53 | -28 | 6.18 |
| 14.0 | 0.85 | -44 | -0.96 | 0.895 | -161 | -17.86 | 0.128 | -145 | 0.58 | -42 | 5.62 |
| 15.0 | 0.86 | -55 | -2.06 | 0.789 | -177 | -18.13 | 0.124 | -156 | 0.62 | -57 | 5.04 |
| 16.0 | 0.85 | -72 | -3.09 | 0.701 | 166 | -18.13 | 0.124 | -168 | 0.65 | -70 | 3.86 |
| 17.0 | 0.85 | -88 | -4.22 | 0.615 | 149 | -18.06 | 0.125 | 177 | 0.68 | -85 | 3.00 |
| 18.0 | 0.88 | -101 | -5.71 | 0.518 | 133 | -18.94 | 0.113 | 165 | 0.71 | -103 | 2.52 |

### ATF-34143 Typical Noise Parameters

$V_{DS} = 3\,V$, $I_{DS} = 20\,mA$

| Freq. GHz | $F_{min}$ dB | $\Gamma_{opt}$ Mag. | Ang. | $R_n/50$ - | $G_a$ dB |
|---|---|---|---|---|---|
| 0.5 | 0.10 | 0.90 | 13 | 0.16 | 21.8 |
| 0.9 | 0.11 | 0.85 | 27 | 0.14 | 18.3 |
| 1.0 | 0.11 | 0.84 | 31 | 0.13 | 17.8 |
| 1.5 | 0.14 | 0.77 | 48 | 0.11 | 16.4 |
| 1.8 | 0.17 | 0.74 | 57 | 0.10 | 16.0 |
| 2.0 | 0.19 | 0.71 | 66 | 0.09 | 15.6 |
| 2.5 | 0.23 | 0.65 | 83 | 0.07 | 14.8 |
| 3.0 | 0.29 | 0.59 | 102 | 0.06 | 14.0 |
| 4.0 | 0.42 | 0.51 | 138 | 0.03 | 12.6 |
| 5.0 | 0.54 | 0.45 | 174 | 0.03 | 11.4 |
| 6.0 | 0.67 | 0.42 | -151 | 0.05 | 10.3 |
| 7.0 | 0.79 | 0.42 | -118 | 0.10 | 9.4 |
| 8.0 | 0.92 | 0.45 | -88 | 0.18 | 8.6 |
| 9.0 | 1.04 | 0.51 | -63 | 0.30 | 8.0 |
| 10.0 | 1.16 | 0.61 | -43 | 0.46 | 7.5 |
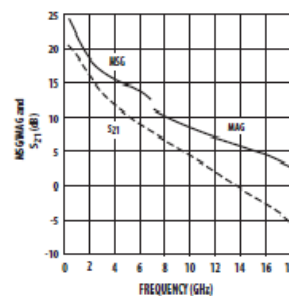


Figure 23. MSG/MAG and $|S_{21}|^2$ vs. Frequency at 3 V, 20 mA.

**Notes:**
1. Fmin values at 2 GHz and higher are based on measurements while the Fmins below 2 GHz have been extrapolated. The Fmin values are based on a set of 16 noise figure measurements made at 16 different impedances using an ATN NP5 test system. From these measurements a true Fmin is calculated. Refer to the noise parameter application section for more information.
2. S and noise parameters are measured on a microstrip line made on 0.025 inch thick alumina carrier. The input reference plane is at the end of the gate lead. The output reference plane is at the end of the drain lead. The parameters include the effect of four plated through via holes connecting source landing pads on top of the test carrier to the microstrip ground plane on the bottom side of the carrier. Two 0.020 inch diameter via holes are placed within 0.010 inch from each source lead contact point, one via on each side of that point.

7

## ATF-34143 Typical Scattering Parameters, $V_{DS} = 3\,V$, $I_{DS} = 40\,mA$

| Freq. GHz | $S_{11}$ Mag. | Ang. | dB | $S_{21}$ Mag. | Ang. | dB | $S_{12}$ Mag. | Ang. | $S_{22}$ Mag. | Ang. | MSG/MAG dB |
|---|---|---|---|---|---|---|---|---|---|---|---|
| 0.5 | 0.96 | -40 | 21.32 | 11.645 | 151 | -30.46 | 0.030 | 68 | 0.29 | -43 | 25.89 |
| 0.8 | 0.89 | -64 | 20.79 | 10.950 | 135 | -27.33 | 0.043 | 56 | 0.24 | -70 | 24.06 |
| 1.0 | 0.85 | -81 | 19.96 | 9.956 | 124 | -25.68 | 0.052 | 49 | 0.24 | -88 | 22.82 |
| 1.5 | 0.79 | -109 | 18.29 | 8.209 | 104 | -23.61 | 0.066 | 36 | 0.23 | -118 | 20.95 |
| 1.8 | 0.76 | -121 | 17.50 | 7.495 | 96 | -22.97 | 0.071 | 32 | 0.23 | -130 | 20.24 |
| 2.0 | 0.74 | -131 | 16.75 | 6.876 | 88 | -22.38 | 0.076 | 27 | 0.22 | -141 | 19.57 |
| 2.5 | 0.70 | -150 | 15.39 | 5.880 | 74 | -21.51 | 0.084 | 19 | 0.22 | -160 | 18.45 |
| 3.0 | 0.67 | -167 | 14.19 | 5.120 | 61 | -20.92 | 0.090 | 12 | 0.22 | -176 | 17.55 |
| 4.0 | 0.64 | 162 | 12.18 | 4.063 | 38 | -19.83 | 0.102 | -1 | 0.21 | 157 | 16.00 |
| 5.0 | 0.64 | 135 | 10.54 | 3.365 | 16 | -19.02 | 0.112 | -14 | 0.22 | 131 | 14.78 |
| 6.0 | 0.65 | 111 | 9.15 | 2.867 | -5 | -18.34 | 0.121 | -28 | 0.24 | 105 | 12.91 |
| 7.0 | 0.66 | 87 | 7.80 | 2.454 | -26 | -17.86 | 0.128 | -42 | 0.28 | 81 | 11.03 |
| 8.0 | 0.69 | 65 | 6.55 | 2.125 | -46 | -17.46 | 0.134 | -55 | 0.32 | 60 | 9.93 |
| 9.0 | 0.73 | 46 | 5.33 | 1.848 | -65 | -17.20 | 0.138 | -69 | 0.37 | 40 | 9.07 |
| 10.0 | 0.76 | 28 | 4.33 | 1.647 | -84 | -16.83 | 0.144 | -84 | 0.41 | 23 | 8.59 |
| 11.0 | 0.78 | 9 | 3.30 | 1.462 | -104 | -16.65 | 0.147 | -99 | 0.45 | 5 | 7.84 |
| 12.0 | 0.80 | -11 | 2.15 | 1.281 | -123 | -16.65 | 0.147 | -114 | 0.50 | -14 | 7.15 |
| 13.0 | 0.83 | -30 | 0.79 | 1.095 | -142 | -17.08 | 0.140 | -130 | 0.55 | -31 | 6.50 |
| 14.0 | 0.86 | -44 | -0.53 | 0.941 | -158 | -17.52 | 0.133 | -142 | 0.60 | -45 | 5.96 |
| 15.0 | 0.87 | -56 | -1.61 | 0.831 | -174 | -17.72 | 0.130 | -154 | 0.64 | -59 | 5.39 |
| 16.0 | 0.86 | -72 | -2.60 | 0.741 | 169 | -17.72 | 0.130 | -166 | 0.66 | -73 | 4.21 |
| 17.0 | 0.86 | -88 | -3.72 | 0.652 | 153 | -17.79 | 0.129 | 179 | 0.69 | -88 | 3.43 |
| 18.0 | 0.88 | -102 | -5.15 | 0.553 | 137 | -18.64 | 0.117 | 166 | 0.72 | -105 | 2.95 |

## ATF-34143 Typical Noise Parameters

$V_{DS} = 3\,V$, $I_{DS} = 40\,mA$

| Freq. GHz | $F_{min}$ dB | $\Gamma_{opt}$ Mag. | Ang. | $R_{n/50}$ - | $G_a$ dB |
|---|---|---|---|---|---|
| 0.5 | 0.10 | 0.87 | 13 | 0.16 | 23.0 |
| 0.9 | 0.13 | 0.82 | 28 | 0.13 | 19.6 |
| 1.0 | 0.14 | 0.80 | 32 | 0.13 | 19.2 |
| 1.5 | 0.17 | 0.73 | 50 | 0.1 | 17.7 |
| 1.8 | 0.21 | 0.70 | 61 | 0.09 | 17.1 |
| 2.0 | 0.23 | 0.66 | 68 | 0.08 | 16.7 |
| 2.5 | 0.29 | 0.60 | 87 | 0.06 | 15.8 |
| 3.0 | 0.35 | 0.54 | 106 | 0.05 | 14.9 |
| 4.0 | 0.47 | 0.46 | 144 | 0.03 | 13.4 |
| 5.0 | 0.6 | 0.41 | -178 | 0.03 | 12.1 |
| 6.0 | 0.72 | 0.39 | -142 | 0.06 | 10.9 |
| 7.0 | 0.85 | 0.41 | -109 | 0.12 | 9.9 |
| 8.0 | 0.97 | 0.45 | -80 | 0.21 | 9.1 |
| 9.0 | 1.09 | 0.52 | -56 | 0.34 | 8.4 |
| 10.0 | 1.22 | 0.61 | -39 | 0.50 | 8.0 |
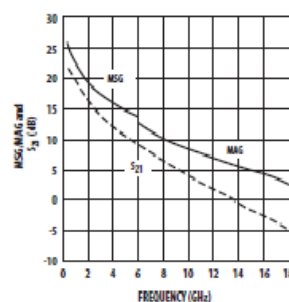


Figure 24. MSG/MAG and $|S_{21}|^2$ vs. Frequency at 3 V, 40 mA.

**Notes:**

1. Fmin values at 2 GHz and higher are based on measurements while the Fmins below 2 GHz have been extrapolated. The Fmin values are based on a set of 16 noise figure measurements made at 16 different impedances using an ATN NP5 test system. From these measurements a true Fmin is calculated. Refer to the noise parameter application section for more information.

2. S and noise parameters are measured on a microstrip line made on 0.025 inch thick alumina carrier. The input reference plane is at the end of the gate lead. The output reference plane is at the end of the drain lead. The parameters include the effect of four plated through via holes connecting source landing pads on top of the test carrier to the microstrip ground plane on the bottom side of the carrier. Two 0.020 inch diameter via holes are placed within 0.010 inch from each source lead contact point, one via on each side of that point.

## ATF-34143 Typical Scattering Parameters, $V_{DS} = 4$ V, $I_{DS} = 40$ mA

| Freq. GHz | $S_{11}$ Mag. | Ang. | dB | $S_{21}$ Mag. | Ang. | dB | $S_{12}$ Mag. | Ang. | $S_{22}$ Mag. | Ang. | MSG/MAG dB |
|---|---|---|---|---|---|---|---|---|---|---|---|
| 0.5 | 0.95 | -40 | 21.56 | 11.973 | 151 | 0.03 | 0.030 | 68 | 0.33 | -39 | 26.01 |
| 0.8 | 0.89 | -65 | 21.02 | 11.252 | 135 | 0.04 | 0.042 | 56 | 0.27 | -63 | 24.28 |
| 1.0 | 0.85 | -82 | 20.19 | 10.217 | 123 | 0.05 | 0.051 | 48 | 0.26 | -80 | 23.02 |
| 1.5 | 0.78 | -109 | 18.49 | 8.405 | 104 | 0.06 | 0.064 | 36 | 0.24 | -109 | 21.18 |
| 1.8 | 0.73 | -131 | 16.93 | 7.024 | 87 | 0.07 | 0.074 | 27 | 0.22 | -131 | 20.46 |
| 2.0 | 0.70 | -150 | 15.57 | 6.002 | 73 | 0.08 | 0.081 | 19 | 0.21 | -150 | 19.77 |
| 2.5 | 0.67 | -167 | 14.36 | 5.223 | 61 | 0.09 | 0.087 | 12 | 0.20 | -167 | 18.70 |
| 3.0 | 0.64 | 162 | 12.34 | 4.141 | 37 | 0.10 | 0.098 | -1 | 0.19 | 165 | 17.75 |
| 4.0 | 0.63 | 135 | 10.70 | 3.428 | 16 | 0.11 | 0.108 | -13 | 0.20 | 138 | 16.26 |
| 5.0 | 0.64 | 111 | 9.32 | 2.923 | -6 | 0.12 | 0.117 | -27 | 0.21 | 111 | 15.02 |
| 6.0 | 0.66 | 87 | 7.98 | 2.506 | -26 | 0.12 | 0.124 | -41 | 0.24 | 86 | 12.93 |
| 7.0 | 0.69 | 65 | 6.74 | 2.173 | -46 | 0.13 | 0.130 | -54 | 0.29 | 63 | 11.14 |
| 8.0 | 0.72 | 47 | 5.55 | 1.894 | -65 | 0.13 | 0.134 | -68 | 0.34 | 42 | 10.09 |
| 9.0 | 0.76 | 28 | 4.55 | 1.689 | -85 | 0.14 | 0.141 | -82 | 0.38 | 26 | 9.24 |
| 10.0 | 0.78 | 9 | 3.53 | 1.501 | -104 | 0.15 | 0.145 | -97 | 0.42 | 8 | 8.79 |
| 11.0 | 0.80 | -11 | 2.39 | 1.317 | -124 | 0.15 | 0.145 | -113 | 0.47 | -11 | 8.09 |
| 12.0 | 0.84 | -29 | 1.02 | 1.125 | -143 | 0.14 | 0.140 | -128 | 0.53 | -29 | 7.35 |
| 13.0 | 0.86 | -44 | -0.30 | 0.966 | -160 | 0.13 | 0.133 | -141 | 0.58 | -43 | 6.76 |
| 14.0 | 0.87 | -56 | -1.38 | 0.853 | -176 | 0.13 | 0.130 | -152 | 0.62 | -58 | 6.19 |
| 15.0 | 0.86 | -72 | -2.40 | 0.759 | 167 | 0.13 | 0.131 | -165 | 0.65 | -71 | 5.62 |
| 16.0 | 0.86 | -88 | -3.53 | 0.666 | 151 | 0.13 | 0.130 | -180 | 0.68 | -86 | 4.43 |
| 17.0 | 0.89 | -102 | -4.99 | 0.563 | 134 | 0.12 | 0.119 | 168 | 0.71 | -103 | 3.60 |
| 18.0 | 0.89 | -101.85 | -4.99 | 0.563 | 134 | 0.12 | 0.119 | 168 | 0.71 | -103 | 3.15 |

## ATF-34143 Typical Noise Parameters

$V_{DS} = 4$ V, $I_{DS} = 40$ mA

| Freq. GHz | $F_{min}$ dB | $\Gamma_{opt}$ Mag. | Ang. | $R_{n/50}$ - | $G_a$ dB |
|---|---|---|---|---|---|
| 0.5 | 0.10 | 0.87 | 13 | 0.16 | 22.8 |
| 0.9 | 0.13 | 0.82 | 27 | 0.14 | 19.4 |
| 1.0 | 0.14 | 0.80 | 31 | 0.13 | 18.9 |
| 1.5 | 0.17 | 0.73 | 49 | 0.11 | 17.4 |
| 1.8 | 0.20 | 0.70 | 60 | 0.10 | 16.9 |
| 2.0 | 0.22 | 0.66 | 67 | 0.09 | 16.4 |
| 2.5 | 0.28 | 0.60 | 85 | 0.07 | 15.6 |
| 3.0 | 0.34 | 0.54 | 104 | 0.05 | 14.8 |
| 4.0 | 0.45 | 0.45 | 142 | 0.03 | 13.3 |
| 5.0 | 0.57 | 0.40 | 180 | 0.03 | 12.0 |
| 6.0 | 0.69 | 0.38 | -144 | 0.05 | 10.9 |
| 7.0 | 0.81 | 0.39 | -111 | 0.11 | 9.9 |
| 8.0 | 0.94 | 0.43 | -82 | 0.20 | 9.1 |
| 9.0 | 1.06 | 0.51 | -57 | 0.32 | 8.5 |
| 10.0 | 1.19 | 0.62 | -40 | 0.47 | 8.1 |
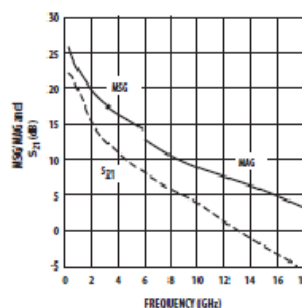


Figure 25. MSG/MAG and $|S_{21}|^2$ vs. Frequency at 4 V, 40 mA.

**Notes:**
1. Fmin values at 2 GHz and higher are based on measurements while the Fmins below 2 GHz have been extrapolated. The Fmin values are based on a set of 16 noise figure measurements made at 16 different impedances using an ATN NP5 test system. From these measurements a true Fmin is calculated. Refer to the noise parameter application section for more information.
2. S and noise parameters are measured on a microstrip line made on 0.025 inch thick alumina carrier. The input reference plane is at the end of the gate lead. The output reference plane is at the end of the drain lead. The parameters include the effect of four plated through via holes connecting source landing pads on top of the test carrier to the microstrip ground plane on the bottom side of the carrier. Two 0.020 inch diameter via holes are placed within 0.010 inch from each source lead contact point, one via on each side of that point.

**ATF-34143 Typical Scattering Parameters, $V_{DS} = 4\,V$, $I_{DS} = 60\,mA$**

| Freq. GHz | $S_{11}$ Mag. | Ang. | dB | $S_{21}$ Mag. | Ang. | dB | $S_{12}$ Mag. | Ang. | $S_{22}$ Mag. | Ang. | MSG/MAG dB |
|---|---|---|---|---|---|---|---|---|---|---|---|
| 0.5 | 0.95 | -41 | 21.91 | 12.454 | 150 | -31.06 | 0.028 | 68 | 0.29 | -41 | 26.48 |
| 0.8 | 0.89 | -65 | 21.33 | 11.654 | 134 | -28.18 | 0.039 | 57 | 0.24 | -67 | 24.75 |
| 1.0 | 0.85 | -83 | 20.46 | 10.549 | 123 | -26.56 | 0.047 | 49 | 0.23 | -84 | 23.51 |
| 1.5 | 0.78 | -111 | 18.74 | 8.646 | 103 | -24.44 | 0.060 | 38 | 0.21 | -114 | 21.59 |
| 1.8 | 0.75 | -122 | 17.92 | 7.873 | 95 | -23.74 | 0.065 | 33 | 0.21 | -125 | 20.83 |
| 2.0 | 0.73 | -133 | 17.16 | 7.207 | 87 | -23.22 | 0.069 | 29 | 0.20 | -136 | 20.19 |
| 2.5 | 0.69 | -151 | 15.78 | 6.149 | 73 | -22.38 | 0.076 | 22 | 0.19 | -155 | 19.08 |
| 3.0 | 0.67 | -168 | 14.56 | 5.345 | 60 | -21.62 | 0.083 | 15 | 0.19 | -171 | 18.09 |
| 4.0 | 0.64 | 161 | 12.53 | 4.232 | 37 | -20.54 | 0.094 | 3 | 0.18 | 162 | 16.53 |
| 5.0 | 0.63 | 134 | 10.88 | 3.501 | 16 | -19.58 | 0.105 | -10 | 0.19 | 135 | 15.23 |
| 6.0 | 0.64 | 111 | 9.49 | 2.983 | -5 | -18.79 | 0.115 | -24 | 0.21 | 109 | 12.89 |
| 7.0 | 0.66 | 86 | 8.15 | 2.557 | -26 | -18.27 | 0.122 | -38 | 0.24 | 84 | 11.22 |
| 8.0 | 0.69 | 65 | 6.92 | 2.217 | -46 | -17.79 | 0.129 | -51 | 0.28 | 62 | 10.21 |
| 9.0 | 0.73 | 46 | 5.72 | 1.932 | -65 | -17.46 | 0.134 | -65 | 0.33 | 42 | 9.36 |
| 10.0 | 0.76 | 28 | 4.73 | 1.723 | -84 | -16.95 | 0.142 | -79 | 0.38 | 25 | 8.94 |
| 11.0 | 0.78 | 9 | 3.70 | 1.531 | -104 | -16.71 | 0.146 | -94 | 0.42 | 7 | 8.23 |
| 12.0 | 0.81 | -11 | 2.57 | 1.344 | -124 | -16.71 | 0.146 | -111 | 0.47 | -12 | 7.56 |
| 13.0 | 0.84 | -30 | 1.20 | 1.148 | -143 | -17.02 | 0.141 | -126 | 0.52 | -29 | 6.94 |
| 14.0 | 0.86 | -44 | -0.12 | 0.986 | -159 | -17.46 | 0.134 | -139 | 0.58 | -43 | 6.37 |
| 15.0 | 0.87 | -56 | -1.21 | 0.870 | -175 | -17.59 | 0.132 | -150 | 0.62 | -58 | 5.78 |
| 16.0 | 0.86 | -72 | -2.21 | 0.775 | 168 | -17.59 | 0.132 | -163 | 0.65 | -71 | 4.60 |
| 17.0 | 0.86 | -88 | -3.35 | 0.680 | 151 | -17.65 | 0.131 | -178 | 0.68 | -86 | 3.79 |
| 18.0 | 0.89 | -101.99 | -4.81 | 0.575 | 135 | -18.42 | 0.120 | 169 | 0.71 | -104 | 3.33 |

**ATF-34143 Typical Noise Parameters**

$V_{DS} = 4\,V$, $I_{DS} = 60\,mA$

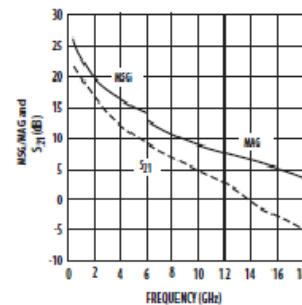| Freq. GHz | $F_{min}$ dB | $\Gamma_{opt}$ Mag. | Ang. | $R_{n}/50$ - | $G_a$ dB |
|---|---|---|---|---|---|
| 0.5 | 0.11 | 0.84 | 15 | 0.14 | 24.5 |
| 0.9 | 0.14 | 0.78 | 30 | 0.12 | 20.7 |
| 1.0 | 0.15 | 0.77 | 34 | 0.12 | 20.2 |
| 1.5 | 0.20 | 0.69 | 53 | 0.10 | 18.5 |
| 1.8 | 0.23 | 0.66 | 62 | 0.10 | 17.7 |
| 2.0 | 0.26 | 0.62 | 72 | 0.09 | 17.2 |
| 2.5 | 0.33 | 0.55 | 91 | 0.07 | 16.3 |
| 3.0 | 0.39 | 0.50 | 111 | 0.05 | 15.4 |
| 4.0 | 0.53 | 0.43 | 149 | 0.03 | 13.7 |
| 5.0 | 0.67 | 0.39 | -173 | 0.04 | 12.3 |
| 6.0 | 0.81 | 0.39 | -137 | 0.07 | 11.1 |
| 7.0 | 0.96 | 0.42 | -104 | 0.14 | 10.0 |
| 8.0 | 1.10 | 0.47 | -76 | 0.26 | 9.2 |
| 9.0 | 1.25 | 0.54 | -53 | 0.41 | 8.6 |
| 10.0 | 1.39 | 0.62 | -37 | 0.60 | 8.2 |



Figure 26. MSG/MAG and $|S_{21}|^2$ vs. Frequency at 4 V, 60 mA.

**Notes:**
1. Fmin values at 2 GHz and higher are based on measurements while the Fmins below 2 GHz have been extrapolated. The Fmin values are based on a set of 16 noise figure measurements made at 16 different impedances using an ATN NP5 test system. From these measurements a true Fmin is calculated. Refer to the noise parameter application section for more information.
2. S and noise parameters are measured on a microstrip line made on 0.025 inch thick alumina carrier. The input reference plane is at the end of the gate lead. The output reference plane is at the end of the drain lead. The parameters include the effect of four plated through via holes connecting source landing pads on top of the test carrier to the microstrip ground plane on the bottom side of the carrier. Two 0.020 inch diameter via holes are placed within 0.010 inch from each source lead contact point, one via on each side of that point.

## Noise Parameter Applications Information

$F_{min}$ values at 2 GHz and higher are based on measurements while the $F_{mins}$ below 2 GHz have been extrapolated. The $F_{min}$ values are based on a set of 16 noise figure measurements made at 16 different impedances using an ATN NP5 test system. From these measurements, a true $F_{min}$ is calculated. $F_{min}$ represents the true minimum noise figure of the device when the device is presented with an impedance matching network that transforms the source impedance, typically 50Ω, to an impedance represented by the reflection coefficient $\Gamma_o$. The designer must design a matching network that will present $\Gamma_o$ to the device with minimal associated circuit losses. The noise figure of the completed amplifier is equal to the noise figure of the device plus the losses of the matching network preceding the device. The noise figure of the device is equal to $F_{min}$ only when the device is presented with $\Gamma_o$. If the reflection coefficient of the matching network is other than $\Gamma_o$, then the noise figure of the device will be greater than $F_{min}$ based on the following equation.
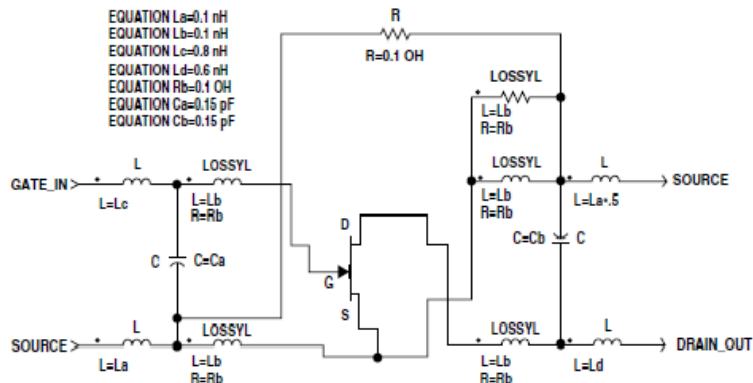
$$NF = F_{min} + 4 R_n \frac{|\Gamma_s - \Gamma_o|^2}{Zo \; (|1 + \Gamma_o|^2)(1 - \Gamma_s|^2)}$$

Where $R_n/Z_o$ is the normalized noise resistance, $\Gamma_o$ is the optimum reflection coefficient required to produce $F_{min}$ and $\Gamma_s$ is the reflection coefficient of the source impedance actually presented to the device. The losses of the matching networks are non-zero and they will also add to the noise figure of the device creating a higher amplifier noise figure. The losses of the matching networks are related to the Q of the components and associated printed circuit board loss. $\Gamma_o$ is typically fairly low at higher frequencies and increases as frequency is lowered. Larger gate width devices will typically have a lower $\Gamma_o$ as compared to narrower gate width devices.

Typically for FETs, the higher $\Gamma_o$ usually infers that an impedance much higher than 50Ω is required for the device to produce $F_{min}$. At VHF frequencies and even lower L Band frequencies, the required impedance can be in the vicinity of several thousand ohms. Matching to such a high impedance requires very hi-Q components in order to minimize circuit losses. As an example at 900 MHz, when airwwound coils (Q > 100) are used for matching networks, the loss can still be up to 0.25 dB which will add directly to the noise figure of the device. Using muiltilayer molded inductors with Qs in the 30 to 50 range results in additional loss over the airwound coil. Losses as high as 0.5 dB or greater add to the typical 0.15 dB $F_{min}$ of the device creating an amplifier noise figure of nearly 0.65 dB. A discussion concerning calculated and measured circuit losses and their effect on amplifier noise figure is covered in Avago Application 1085.

## ATF-34143 SC-70 4 Lead, High Frequency Nonlinear Model
### Optimized for 0.1–6.0 GHz

EQUATION La=0.1 nH
EQUATION Lb=0.1 nH
EQUATION Lc=0.8 nH
EQUATION Ld=0.6 nH
EQUATION Rb=0.1 OH
EQUATION Ca=0.15 pF
EQUATION Cb=0.15 pF



This model can be used as a design tool. It has been tested on MDS for various specifications. However, for more precise and accurate design, please refer to the measured data in this data sheet. For future improvements Avago reserves the right to change these models without prior notice.

## ATF-34143 Die Model

```
                    * STATZ MESFET MODEL *
                        MODEL = FET

IDS model        Gate model      Parasitics      Breakdown       Noise
NFET=yes         DELTA=.2        RG=1            GSFWD=1         FNC=01e+6
PFET=            GSCAP=3         RD=Rd           GSREV=0         R=.17
IDSMOD=3         CGS=cgs pF      RS=Rs           GDFWD=1         P=.65
VTO=−0.95        GDCAP=3         LG=Lg nH        GDREV=0         C=.2
BETA= Beta       GCD=Cgd pF      LD=Ld nH        VJR=1
LAMBDA=0.09                      LS=Ls nH        IS=1 nA
ALPHA=4.0                        CDS=Cds pF      IR=1 nA
B=0.8                            CRF=.1          IMAX=.1
TNOM=27                          RC=Rc           XTI=
IDSTC=                                           N=
VBI=.7                                           EG=
```

### Model scal factors (W=FET width in microns)

EQUATION Cds=0.01•W/200
EQUATION Beta=0.06•W/200
EQUATION Rd=200/W

EQUATION Rs=.5•200/W
EQUATION Cgs=0.2•W/200

EQUATION Cgd=0.04•W/200
EQUATION Lg=0.03•200/W

EQUATION Ld=0.03•200/W
EQUATION Ls=0.01•200/W
EQUATION Rc=500•200/W



NFETMESFET

MODEL=FET

W=800 μm

12
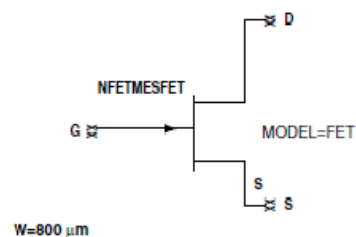
**Part Number Ordering Information**

| Part Number | No. of Devices | Container |
|---|---|---|
| ATF-34143-TR1G | 3000 | 7" Reel |
| ATF-34143-TR2G | 10000 | 13" Reel |
| ATF-34143-BLKG | 100 | antistatic bag |

**Package Dimensions**
**SC-70 4L/SOT-343**

**Recommended PCB Pad Layout for Avago's SC70 4L/SOT-343 Products**



Dimensions in mm/(inches)
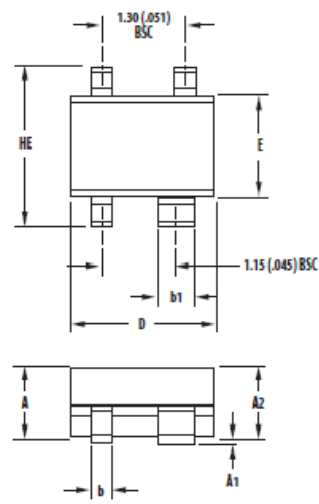
| SYMBOL | DIMENSIONS (mm) | |
|---|---|---|
| | MIN. | MAX. |
| E | 1.15 | 1.35 |
| D | 1.85 | 2.25 |
| HE | 1.80 | 2.40 |
| A | 0.80 | 1.10 |
| A2 | 0.80 | 1.00 |
| A1 | 0.00 | 0.10 |
| b | 0.15 | 0.40 |
| b1 | 0.55 | 0.70 |
| c | 0.10 | 0.20 |
| L | 0.10 | 0.46 |
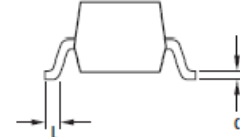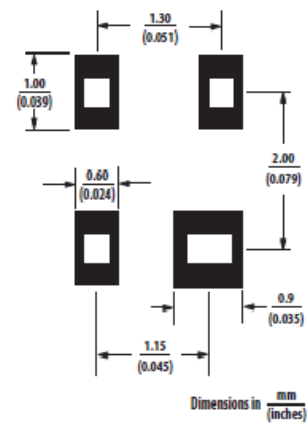
NOTES:
1. All dimensions are in mm.
2. Dimensions are inclusive of plating.
3. Dimensions are exclusive of mold flash & metal burr.
4. All specifications comply to EIAJ SC70.
5. Die is facing up for mold and facing down for trim/form, ie: reverse trim/form.
6. Package surface to be mirror finish.

**Device Orientation**
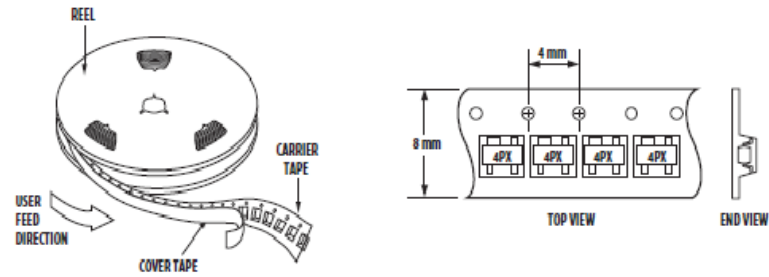


**Tape Dimensions for Outline 4T**
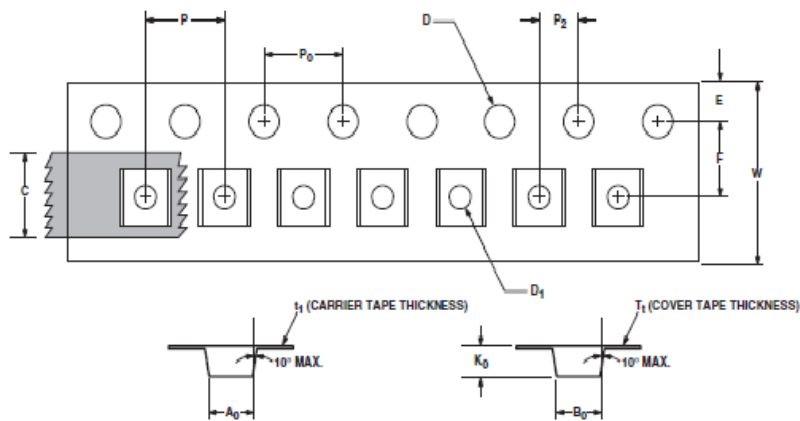


| | DESCRIPTION | SYMBOL | SIZE (mm) | SIZE (INCHES) |
|---|---|---|---|---|
| CAVITY | LENGTH | $A_0$ | 2.40 ± 0.10 | 0.094 ± 0.004 |
| | WIDTH | $B_0$ | 2.40 ± 0.10 | 0.094 ± 0.004 |
| | DEPTH | $K_0$ | 1.20 ± 0.10 | 0.047 ± 0.004 |
| | PITCH | P | 4.00 ± 0.10 | 0.157 ± 0.004 |
| | BOTTOM HOLE DIAMETER | $D_1$ | 1.00 + 0.25 | 0.039 + 0.010 |
| PERFORATION | DIAMETER | D | 1.55 ± 0.10 | 0.061 + 0.002 |
| | PITCH | $P_0$ | 4.00 ± 0.10 | 0.157 ± 0.004 |
| | POSITION | E | 1.75 ± 0.10 | 0.069 ± 0.004 |
| CARRIER TAPE | WIDTH | W | 8.00 + 0.30 - 0.10 | 0.315 + 0.012 |
| | THICKNESS | $t_1$ | 0.254 ± 0.02 | 0.0100 ± 0.0008 |
| COVER TAPE | WIDTH | C | 5.40 ± 0.10 | 0.205 + 0.004 |
| | TAPE THICKNESS | $T_t$ | 0.062 ± 0.001 | 0.0025 ± 0.0004 |
| DISTANCE | CAVITY TO PERFORATION (WIDTH DIRECTION) | F | 3.50 ± 0.05 | 0.138 ± 0.002 |
| | CAVITY TO PERFORATION (LENGTH DIRECTION) | $P_2$ | 2.00 ± 0.05 | 0.079 ± 0.002 |

For product information and a complete list of distributors, please go to our web site: **www.avagotech.com**